PCCP

Crystalline Structure and Thermotropic Behavior of Alkyltrimethylphosphonium Amphiphiles

Journal:	*Physical Chemistry Chemical Physics*
Manuscript ID	Draft
Article Type:	Paper
Date Submitted by the Author:	n/a
Complete List of Authors:	Gamarra, Ana; Universitat Politècnica de Catalunya, Barcelona, Spain Urpí, Lourdes; Universitat Politècnica de Catalunya, Barcelona, Spain Martínez de Ilarduya, Antxon; Universitat Politècnica de Catalunya, Barcelona, Spain Muñoz-Guerra, Sebastián; Universitat Politècnica de Catalunya, Barcelona, Spain

Crystalline Structure and Thermotropic Behavior of Alkyltrimethylphosphonium Amphiphiles

Ana Gamarra, Lourdes Urpí, Antxon Martínez de Ilarduya and Sebastián Muñoz-Guerra*

Departament d'Enginyeria Química, Universitat Politècnica de Catalunya, ETSEIB, Diagonal 647, Barcelona 08028, Spain.

E-mail: sebastian.munoz@upc.edu

Abstract

Quaternary organophosphonium salts bearing long alkyl chains are cationic surfactants of interest for their physical and biological properties. In the present work, the crystal structure and thermotropic behavior of the homologous series of alkyltrimethylphosphonium bromides (*n*ATMP·Br), with the alkyl chain containing *n* even numbers of carbon atoms from 12 to 22, have been examined within the 0-300 ºC range of temperatures. These compounds showed to be resistant to heat up to ~390 ºC. The phases adopted at different temperatures were detected by DSC, and the structural changes involved in the phase transitions have been characterized by simultaneous WAXS and SAXS carried out in real-time, and by polarizing optical microscopy as well. Three or four phases were identified for *n* =12 and 14 or *n*≥ 16 respectively, in agreement with the heat exchange peaks observed by DSC. The phase existing at room temperature (Ph-I) was found to be fully crystalline and its crystal lattice was determined by single-crystal X-ray diffraction methods. Ph-II consisted of a semicrystalline structure that can be categorized as Smectic-B with the crystallized ionic pairs hexagonally arranged in layers and the molten alkyl chain confined in the interlayer space. Ph-II of 12ATMP·Br and 14ATMP·Br directly isotropicized upon heating at ~220 ºC whereas for *n* ≥ 16 it converted into a Smectic-A phase (Ph-III) that needed to be heated above ~240 ºC to become isotropic (Ph-Is). The correlation existing between thermal behavior, phase structure and length of the alkyl side chain has been demonstrated.

Introduction

Tetraalkylphosphonium salts bearing long alkyl chains constitute a family of cationic amphiphiles comparable to the widely known tetraalkylammonium family but that offers superior properties in some aspects. Quaternary organophosphonium compounds are particularly attractive as ionic liquids because they display high thermal stability[1] and may be designed with a wide diversity of structures, some of them being able to melt at sub-ambient temperatures.[2] Their applications as solvents,[3–5] phase transfer catalysts,[6] or exfoliation agents for nanoclays,[7–9] among others have been recently explored for some of these compounds. They are also interesting as building blocks in the design of antimicrobial materials since it has been proved

that they are less cytotoxic than organoammonium compounds.[10,11] Nevertheless the research carried out to date on organophosphonium salts, and in particular on tetraalkylphosphonium ones, is much less extensive than on their ammonium analogues so that the knowledge currently available on their structure and properties is relatively limited.[12] Such comparative backwardness is mainly due to the synthesis difficulties associated to phosphorous chemistry as well as to the restricted availability of the trialkylphosphines that are commonly used as starting materials.

The ability of tetraalkylammonium surfactants to form thermotropic mesophases is a well-known fact that has been investigated for a good number of systems.[13] These compounds usually adopt an amphiphilic arrangement with the ammonium-halide ionic pairs aligned in layers and the hydrophobic alkyl chains in a more or less extended conformation filling the interlayer spacing.[14] Tetraalkylphosphonium surfactants are able to take up similar arrangements but covering broader domains of temperatures and displaying higher clearing points.[15] Fortunately, the characterization of the high-temperature phases found in phosphonium surfactants is feasible thanks to the good thermal stability displayed by these systems. Nevertheless, the literature dealing with the structure and thermal behavior of phosphonium-based surfactants is scarce, a meager situation that is evidenced when compared with the vast amount of information that has been amassed on commercialized surfactants based on tetraalkylammonium salts. To the best of our knowledge, the few studies carried out to date on phosphonium-based surfactants concern salts bearing two, three or four long alkyl chains,[15–18] whereas no study has been addressed to examine those containing only one long alkyl chain except that of Kanazawa et al. which was devoted to evaluate the antimicrobial properties of the chloride salts of some of these compounds.[19]

In this paper we wish to report on a series of alkyltrimethylphosphonium bromide surfactants, abbreviated as *n*ATMP·Br (Scheme 1) with the alkyl chain being linear and containing an even number of carbon atoms (*n*) ranging from 12 to 22. The primary purpose of

the work is to provide physicochemical knowledge on the structure and properties of this family of surfactants of potential interest for novel applications, in particular for the synthesis of surfactant-polymer complexes. Comb-like complexes generated by ionic coupling of naturally-occurring polyelectrolytes with ionic surfactants are receiving exceptional attention.[20] Thus complexes made of bacterially produced poly(γ-glutamic acid)[21,22] or certain polyuronic acids[23] and alkyltrimethylammonium soaps have been prepared and demonstrated to be useful for drug encapsulation[24] and also as compatibilizers[25] for bionanocomposites. For the development of new complexes based on alkytrimethylphosphonium surfactants, the structure of these compounds should be determined and their basic properties properly evaluated. This paper includes the synthesis of the *n*ATMP·Br series, the characterization of their thermal transitions, and the structural analysis of the thermotropic phases that they are able to adopt as a function of temperature.

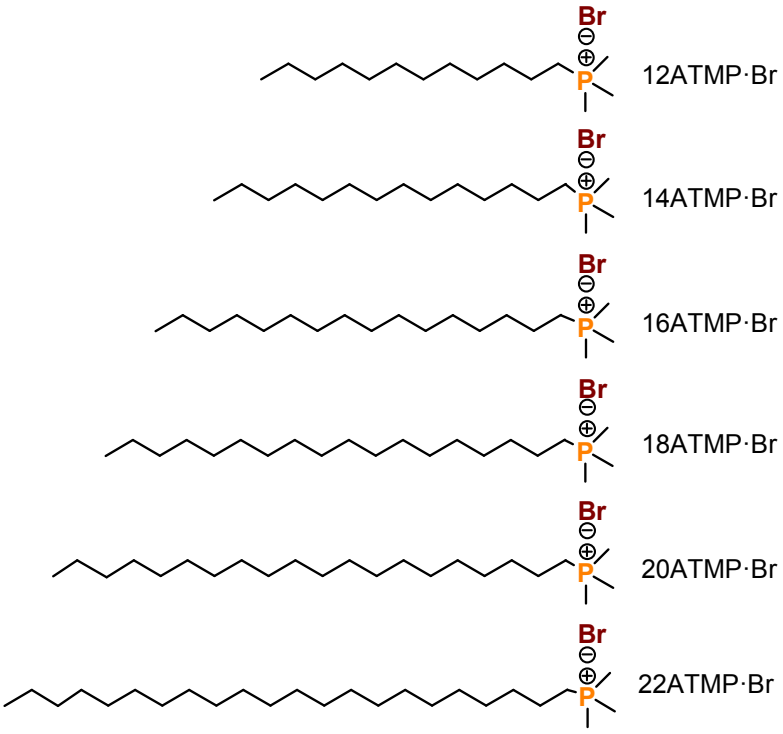

Scheme 1. Chemical formulae of *n*ATMP·Br surfactants.

Experimental

Materials

1-Bromododecane (97%), 1-bromohexadecane (97%), 1-bromooctadecane (96%), 1-bromoeicosane (98%), 1-bromodocosane (96%) and trimethylphosphine solution in toluene (1M) were supplied from Sigma-Aldrich, and 1-bromotetradecane (97%) from Merck. They all were used as received. Solvents were supplied from Panreac and used without further purification.

Synthesis of alkyltrimethylphosphonium bromides

The synthesis of the alkyltrimethylphosphonium surfactants (*n*ATMP·Br) was carried out as follows. 5 mL of a 1.0 M solution of trimethylphosphine (TMP) in toluene (5 mmol) was slowly added to 1-bromoalkane (5.5 mmol) preheated at 80 ºC and under a nitrogen atmosphere. The mixture was then heated in a silicone oil bath up to 116 ºC and maintained at that temperature under stirring for a period of 18 to 24 h depending on the value of *n*. The precipitate formed at the end of the reaction period was collected by filtration. In order to remove the excess of the bromoalkane, the precipitate was repeatedly washed with toluene and then dried under vacuum for 48 h. The *n*ATMP·Br salts were recovered as white powders in yields ranging between 70 and 90%. They all were soluble in a variety of organic solvents such as chloroform and methanol, and also in water at temperatures between 20 ºC and 60 ºC depending on the length of the alkyl chain. Synthesis data of these compounds are given in full detail in the ESI file.

Elemental analysis and spectroscopy

Elemental analyses were carried out at the Servei de Microanàlisi at IQAC (Barcelona). Tests were made in a Flash 1112 elemental microanalyser (A5) which was calibrated with appropriate standards of known composition. C and H contents were determined by the dynamic flash combustion method using He as carrier gas. Results were given in (w/w) percentages and in duplicates.

FT-IR spectra were recorded within the 4000-600 cm^{-1} interval from powder samples on a FT-IR Perkin Elmer Frontier spectrophotometer provided with a universal ATR sampling accessory for solid samples. ^{1}H and ^{13}C NMR spectra were recorded on a Bruker AMX-300 NMR instrument and using TMS as internal reference. The spectra were registered at 300.1 MHz for ^{1}H NMR and at 75.5 MHz for ^{13}C NMR MHz from samples dissolved in deuterated chloroform.

Krafft temperature and critical micelle concentration (*cmc*)

Krafft temperatures (T_{Krafft}) were estimated visually. Samples were prepared as follows: 1% (w/w) mixtures of *n*ATMP·Br in water were heated until dissolution and then cooled down to room temperature and kept in a refrigerator at 5 ºC for 24 hours. The cooled samples were then introduced in a water bath provided with a magnetic stirring and heated up in steps of 1 ºC every 15 min. The temperature at which turbidity disappeared was taken as the approximate Krafft temperature. The *cmc* for *n* = 12, 14 and 16 were determined by ^{1}H NMR following the evolution of the chemical shifts of specific signals of the surfactant with increasing concentration according to the procedure described in the literature.[26,27] Samples were dissolved in D_2O, and ^{1}H NMR spectra were recorded at the selected temperature using the sodium salt of the 3-(trimethylsilyl)-propanesulfonic acid as internal reference.

Thermal measurements

Thermogravimetric analyses were performed under an inert atmosphere with a Perkin-Elmer TGA6 thermobalance at heating rates of 10 ºC·min^{-1} using sample weights of 10-15 mg. Calorimetric measurements were performed with a Perkin-Elmer Pyris DSC instrument calibrated with indium and zinc. Sample weights of about 2–5 mg were used to record heating-cooling cycles at rates of 10 ºC·min^{-1} within the temperature range of -30 to 280 ºC under a nitrogen atmosphere.

X-ray diffraction and optical microscopy

X-ray diffraction (XRD) using conventional light was performed in the "Centres Científics i Tecnològics de la Universitat de Barcelona" (CCiT). XRD patterns were registered at room temperature from powder samples, either coming directly from synthesis or previously heated at selected temperatures. The diffractometer used was a PANalytical X'Pert PRO MPD theta/theta with Cu(K_α) radiation (λ = 0.15418 nm). The reflections collected were those appearing in the 1º ≤ θ ≤ 15º range. Real time X-ray diffraction studies were carried out using X-ray synchrotron radiation at the BL11 beamline (Non-Crystalline Diffraction (NCD), at ALBA (Cerdanyola del Vallès, Barcelona, Spain). Both SAXS and WAXS were taken simultaneously from powder samples subjected to heating-cooling cycles at rates of 10 or 0.5 ºC·min^{-1}. The energy employed corresponded to a 0.10 nm wavelength, and spectra were calibrated with silver behenate (AgBh) and Cr_2O_3 for SAXS and WAXS, respectively.

Optical microscopy was carried out on an Olympus BX51 polarizing optical microscope equipped with a digital camera and a Linkam THMS-600 hot stage provided with a nitrogen gas circulating system to avoid contact with air and humidity. Samples for observation were prepared by casting 1% (w/v) chloroform solutions of the surfactant on a microscope square glass coverslip and the dried film covered with another slide.

Single-crystal analysis

The 12ATMP·Br surfactant was subjected to structural analysis using a monocrystal that was grown by the vapor-diffusion technique at 20 ºC. The applied procedure was as follows: A solution of the surfactant (0.5 mg·mL^{-1}) in $CHCl_3$:EtOAc (90:10) was prepared and distributed in a multi-well plate, which was then placed in a closed chamber and left to evaporate under a EtOAc saturated atmosphere. After several days a unique large monocrystal of 0.45 x 0.14 x 0.10 mm dimensions suitable for XRD analysis was formed. The selected crystal was mounted on a D8 Venture diffractometer provided with a multilayer monochromator Mo-K_α radiation (λ =

0.071073 nm), and the generated scattering was collected with an area detector Photon 100 CMOS. Unit cell parameters were determined from 7111 reflections within the θ range of 2.23° to 25.14°. Intensities of 25,175 reflections collected within the 2.23°-25.39° angular range were measured. The structure was solved by direct methods and refined by least-squared method (SHELXL-2014 program).[28] A detailed description of the methodology used for the structure analysis is given in the ESI file attached to this paper.

Results and discussion

Synthesis and characterization of *n*ATMP·Br

The alkyltrimethylphosphonium bromides (*n*ATMP·Br) studied in this work were synthesized by nucleophilic reaction of trimethylphosphine onto the corresponding alkyl bromide at properly adjusted times and temperatures. Specific conditions used for reaction and yields obtained thence for every *n*ATMP·Br are detailed in Table 1. The elemental composition in carbon and hydrogen of *n*ATMP·Br was checked by combustion analysis and their chemical constitution was ascertained by both FT-IR and NMR spectroscopy. Infrared spectra showed bands at ~990 and ~715 cm^{-1} indicative of the presence of the trimethylphosphonium group[29,30] as well as others at ~2900-2850 and ~1470 cm^{-1} arising from the C-H stretching and bending vibrations respectively whose absorbance increased with the length of the long alkyl chain. ^{1}H and ^{13}C NMR spectra were in full agreement with the structure expected for the *n*ATMP·Br with all the observed signals being properly assigned regarding both chemical shifts and intensities. The whole collection of spectra registered from the *n*ATMP·Br series are reproduced in the ESI file.

As expected, the solubility and aggregation properties of the *n*ATMP·Br series are depending on *n*. The Krafft temperatures (T_{Krafft}) and the critical micellar concentrations (*cmc*) of the surfactants are listed in Table 1. The T_{Krafft} of the phosphonium surfactants are lower than

those displayed by their ammonium analogs[31] with values falling below zero for *n* = 12 and 14. The *cmc* were measured by NMR for those members displaying T_{Krafft} below room temperature, *i.e*. for *n* = 12, 14 and 16. As expected and according to that is observed in other ionic surfactant series, the *cmc* value decreased exponentially as the length of the alkyl chain increased. It is remarkable that the values observed for this series are noticeable lower than those reported for the alkyltrimethylammonium series.[27] A detailed account of the *cmc* determination carried out by the NMR method is given in the ESI file.

Table 1. Synthesis data of *n*ATMP·Br surfactants.

n	*t* (h)	*T* (ºC)	Yield (%)	Elemental analysis[a]		T_{Krafft}[b] (ºC)	*cmc*[c] ($mM \cdot L^{-1}$)
				C (%)	H (%)		
12	16	116	70	55.53 (55.53)	10.50 (10.59)	<0	9.9
14	17	116	80	58.03 (57.92)	10.79 (10.90)	<0	2.7
16	18	116	85	60.06 (59.96)	11.00 (11.16)	15	0.65
18	20	116	70	61.56 (61.73)	11.22 (11.38)	30	n.d
20	22	116	80	63.12 (63.26)	11.37 (11.58)	45	n.d
22	24	116	70	64.70 (64.61)	11.65 (11.75)	55	n.d

[a]In parenthesis, calculated values for the expected compositions. [b]Visually estimated for a 1% (w/w) concentration. [c]Measured by ^{1}H NMR at 25 ºC.

Thermal stability

The TGA traces recorded from *n*ATMP·Br surfactants under an inert atmosphere are depicted in Fig. 1, and the most relevant thermal decomposition parameters measured either directly on these traces or from their derivative curves (ESI file) are listed in Table 2.

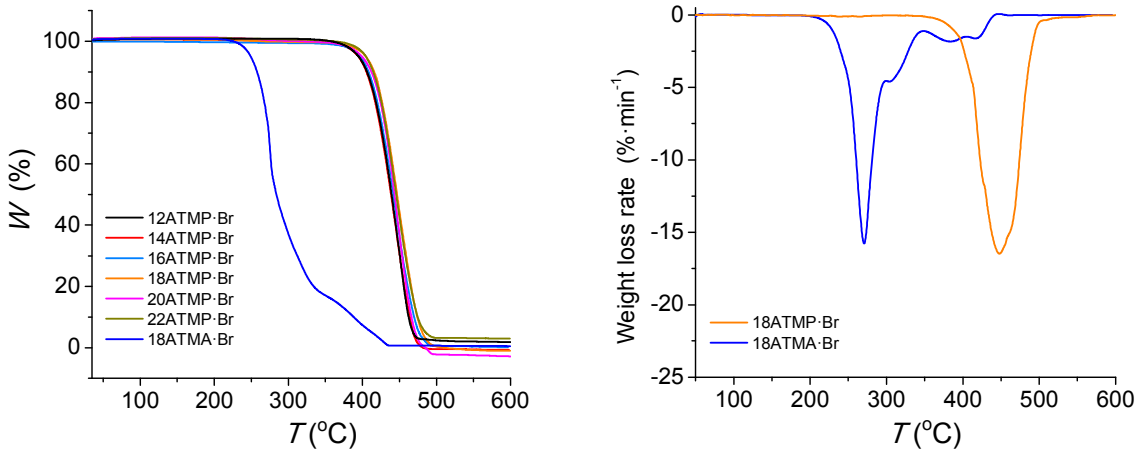

Fig. 1. Left: TGA traces of the *n*ATMP·Br series recorded under a nitrogen atmosphere. The trace produced by octadecyltrimethylammonium bromide (18ATMA·Br) is included for comparison. Right: Compared derivative traces of 18ATMP·Br and 18ATMA·Br.

Decomposition temperatures corresponding to a 5% loss of the initial weight ($^{\circ}T_d$) were above 390 ºC, and maximum decomposition rate temperatures were observed in the 440-445 ºC range with a slight trend towards higher values as the length of the alkyl chain increased. Only one peak is displayed in the derivative plots indicating that decomposition takes place cleanly in one single step with almost negligible residual weight. This behavior contrasts with the thermal decomposition reported for octadecyltrimethylammonium bromide (18ATMA·Br), which displays a $^{\circ}T_d$ below 200 ºC and decomposes through a complex mechanism whose main step takes place at temperatures below 300 ºC.[15] The trace of this compound has been included in Fig.1 for comparison and the complete collection traces of the *n*ATMA·Br series is included in the ESI document. It is precisely the great thermal stability displayed by the *n*ATMP·Br surfactants that makes them particularly appealing for their use as clay modifiers in the design of nanocomposites with high resistance to heat.[32] An isothermal essay carried out with 18ATMP·Br revealed that this compound lost less than 2% of its original weight after heating at 280 ºC for three days under an inert atmosphere (ESI file).

Thermal transitions

The DSC analysis on *n*ATMP·Br was aimed at bringing out the occurrence of thermal transitions, and it consisted of recording three heating-cooling cycles over the -30 to 300 ºC range for each surfactant. The recorded DSC traces are depicted in Fig. 2, and temperatures and enthalpies associated to the heat exchanges observed on the traces are listed in Table 2.

Table 2. Thermal properties of *n*ATMP·Br surfactants.

	TGA[a]			DSC[b]								
				1st Heating			Cooling			2nd Heating		
n	$^{o}T_d$ (ºC)	$^{max}T_d$ (ºC)	*W* (%)	I/II	II/III	III/Is	II/I	III/II	Is/III	I/II	II/III	III/Is
12	395	443	~1	66 (39.0)	← 215 → (12.1)		40 (-14.0)	← 212 → (-11.5)		59 (20.6)	← 214 → (11.5)	
14	395	443	~0	75 (44.7)	← 225 → (11.3)		59 (-13.2)	← 218 → (-11.4)		73 (21.2)	← 225 → (10.9)	
16	398	443	~0	84 (49.5)	228 (10.4)	241 (1.5)	68 (-18.4)	224 (-10.9)	240 (-1.6)	75 (21.2)	228 (10.7)	242 (1.6)
18	399	444	~1	89 (60.6)	227 (10.1)	260 (1.6)	76 (-23.1)	220 (-11.3)	258 (-1.6)	84 (24.3)	227 (10.1)	260 (1.5)
20	400	445	~0	91 (69.2)	223 (10.0)	263 (1.3)	80 (-27.6)	217 (-11.3)	264 (-1.1)	87 (28.9)	224 (10.3)	268 (1.2)
22	405	445	~3	99 (76.0)	225 (10.8)	271 (1.5)	90 (-31.7)	218 (-10.4)	271 (-1.2)	96 (33.5)	225 (10.1)	271 (1.2)

[a] $^{o}T_d$ = onset decomposition temperature for 5% of weight loss; $^{max}T_d$ = maximum rate decomposition temperature; *W* = remaining weight after heating at 600 ºC. [b] Temperatures (ºC) and enthalpies (kJ·mol^{-1}, in parenthesis) observed at heating and cooling for the indicated phase transitions.

Two main endothermal peaks were observed on the first heating traces within the 60-100 ºC and 210-225 ºC ranges, respectively, both of them reappearing after cooling and reheating, and two exothermal peaks were also observed on their respective cooling traces at somewhat lower temperatures. It is noticed that the transition occurring in the low temperature region (below 100 ºC) required a significant supercooling (~10-25 ºC) that steadily enlarged as the length of the alkyl chain diminished, and produced a material showing at the second heating an endothermic peak with the enthalpy reduced in about 30-40% of its initial value. These features strongly suggest that this transition must involve the interconversion between a crystal phase (Ph-I) and a molten phase (Ph-II) through a melting-crystallization process that is homogenously

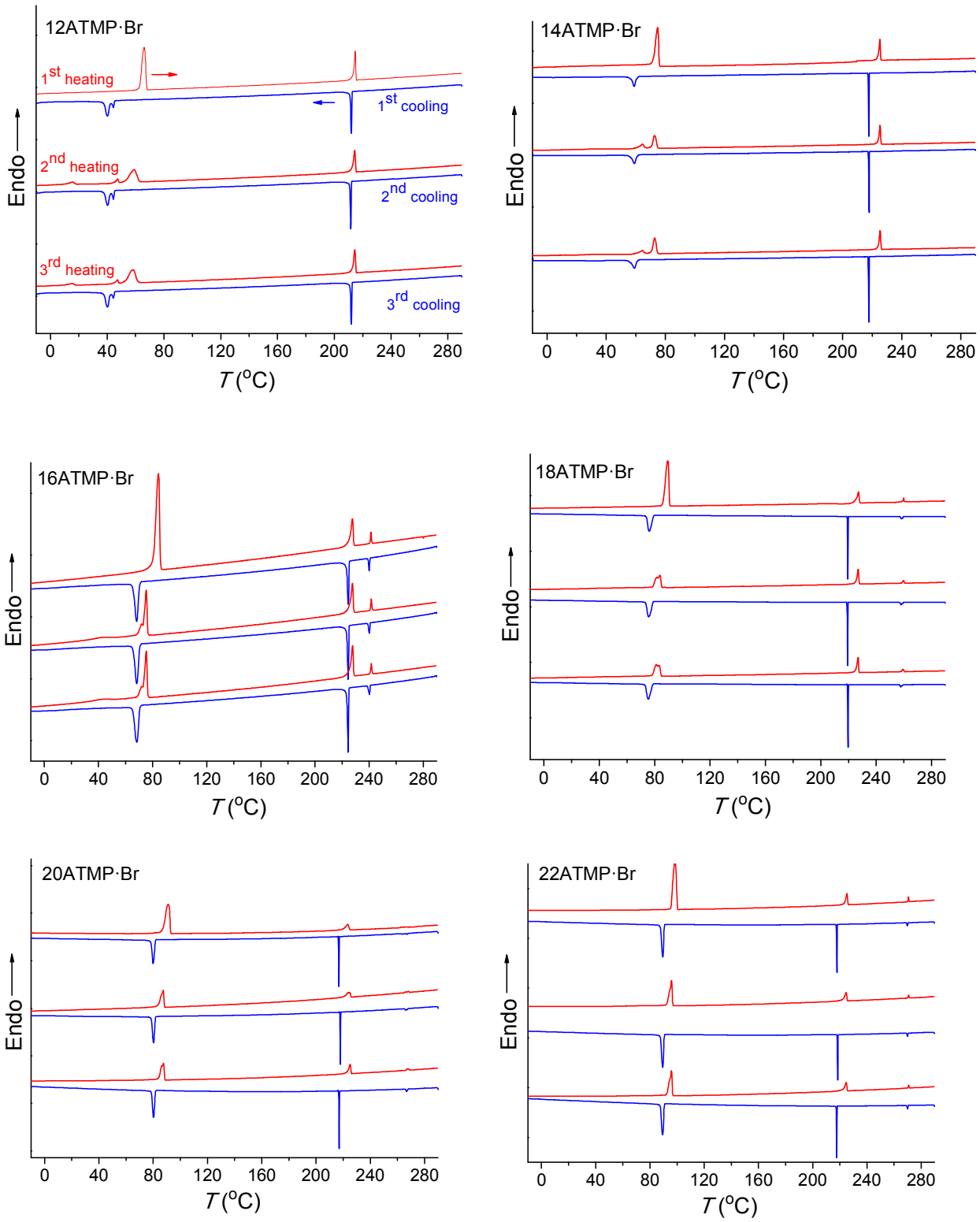

Fig. 2. DSC traces of *n*ATMP·Br at successive heating-cooling cycles over the -30 ºC to 280 ºC interval.

nucleated. Conversely, the second heat exchange taking place above 200 ºC showed almost negligible supercooling, and the initial endothermal peak was almost exactly reproduced in the second heating trace with both position and intensity essentially preserved at the original values. The transition associated to this peaks-pair should imply therefore an interconversion between two liquid-crystal phases (Ph-II and Ph-III) that must be very closely interrelated. In addition to these two transitions, a third endo/exo heat exchange was detectable for *n*ATMP·Br with $n \geq 16$ when heated above 240 ºC. This third transition takes place at temperatures steadily increasing with *n* and involves a very small heat exchange (~1-1.5 $kJ \cdot mol^{-1}$) that is not appreciably depending on *n*, and that reverses without perceivable supercooling. As it will be seen below, this peak is associated to the isotropization of Ph-III taking place in *n*ATMP·Br with $n \geq 16$.

Temperatures, enthalpies and entropies involved in the thermal transitions observed for *n*ATMP·Br are plotted against *n* in Fig.3. The almost linear trend followed by the three parameters as a function of *n* becomes clearly apparent in these plots and the comparative analysis of the plotted data provides insight into the nature of the transitions: a) The sloping linear dependence of the Ph-I/Ph-II transition parameters, both *T* and ΔH, on *n* is consistent with the occurrence of a process entailing the melting/crystallization of the polymethylene chain. b) On the contrary, the invariance observed for these parameters in the Ph-II/Ph-III interconversion indicates that the trimethylphosphonium group must be the counterpart of the surfactant mainly implied in the rearrangement taking place in this transition with the alkyl chain playing an irrelevant role. On the other hand, the linear dependence on *n* of the Ph-III/Ph-Is transition temperature and the very small enthalpy therein involved suggest the occurrence of an entropically driven process leading to the complete disordering of the system. It is interesting to note that extrapolation of the *T*-*n* straight line of Ph-III/Ph-Is to *n* values of 14 and 12 includes the corresponding points of the Ph-II/Ph-III line. It could be therefore interpreted that for these

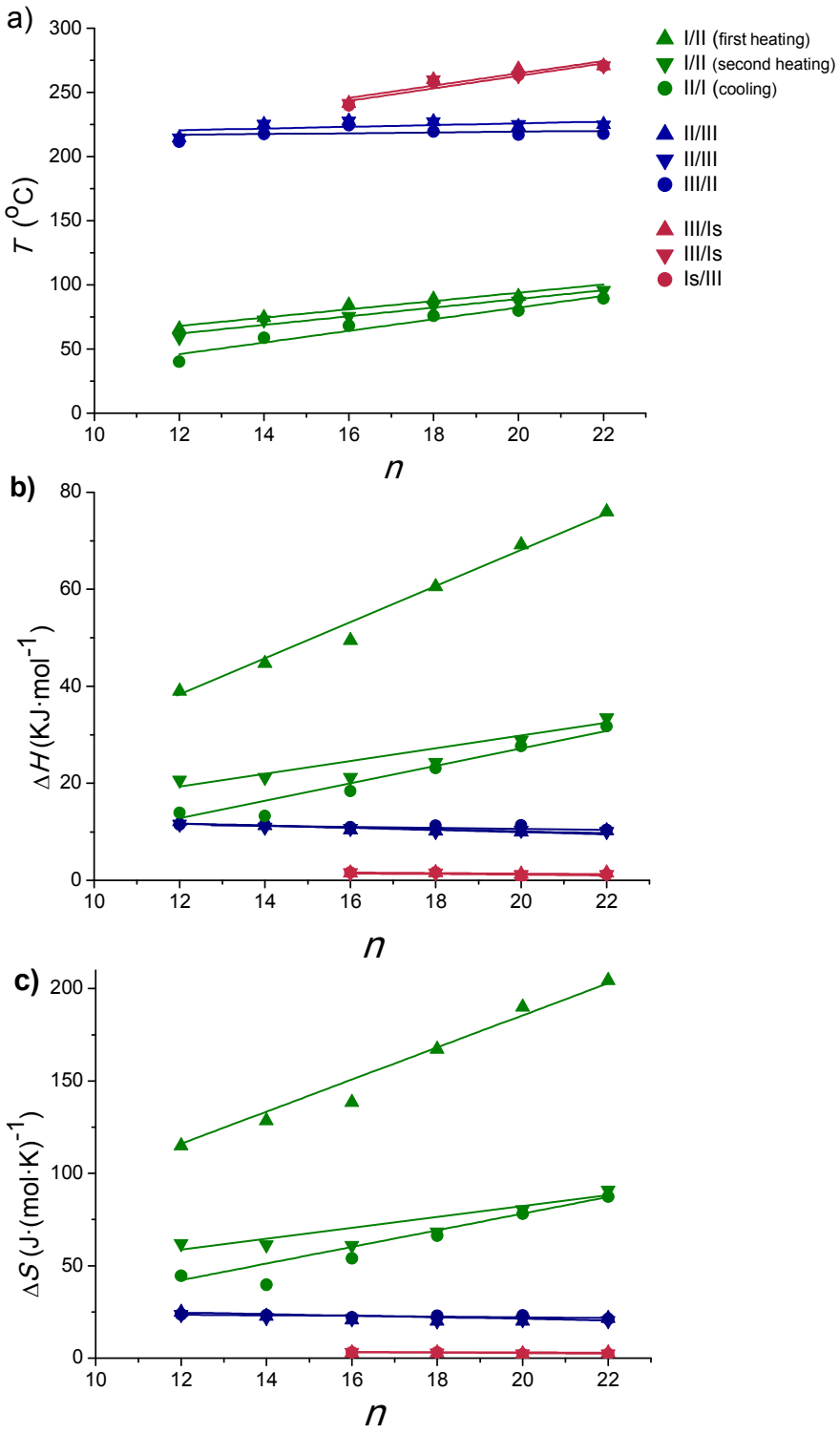

Fig. 3. Phase transition temperatures (a), enthalpies (b) and entropies (c) of *n*ATMP·Br surfactants as a function of *n*. In (b) the Δ*H* negative values registered at cooling are represented in positive for a closer comparison with the Δ*H* values registered at heating.

two surfactants, Ph-II is directly converted into Ph-Is without going through Ph-III; Ph-III is envisaged then as an intermediate phase that has only existence when the alkyl chains are sufficiently long. A scheme of the existence domains of the different phases is depicted in Fig. 4.

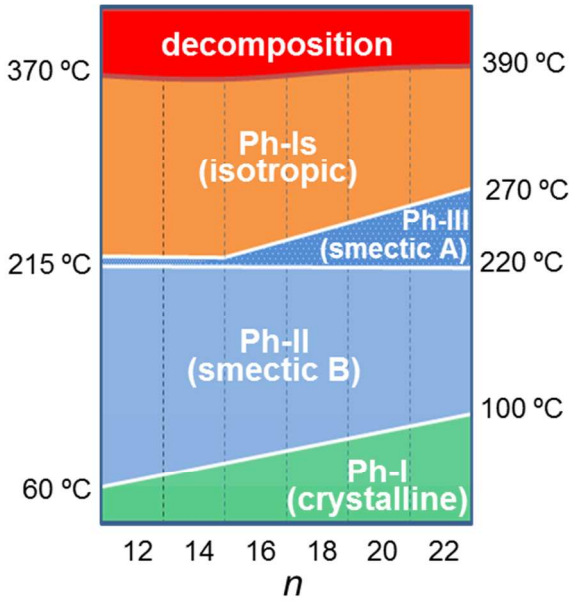

Fig. 4. Domains of existence of *n*ATMP·Br phases. Temperatures are approximately indicated.

Crystal structure of *n*ATMP·Br at room temperature (Phase I)

Phase I (Ph-I) is the phase adopted by *n*ATMP·Br surfactants at room temperature over an existence domain that extends up to 60-100 ºC depending on *n*. The scattering produced by this phase when subjected to X-ray diffraction (XRD) consists of a profile made of multiple discrete peaks characteristic of a crystalline state. In the SAXS region (≥1.5 nm), a very sharp strong peak corresponding to a repeat ranging from 1.8 up to 2.8 nm is conspicuously observed as *n* increases from 12 to 22 (Fig. 5a). According to what is known for other related surfactants as those made of a trimethylammonium group bearing a long polymethylene chain,[33] such spacing is interpreted as arising from the periodical distance (*L*) characteristic of the layered biphasic structure usually adopted by these compounds. On the other hand, the diffraction

observed for *n*ATMP·Br in the WAXS region (~0.7-0.3 nm) consists of a good number of peaks of varying intensity with most of them being shared by the whole series (Fig. 5b), which strongly suggests that the same crystal structure is very probably adopted in all cases. It should be noted that some slight mismatching is more than reasonable to occur since minor deviations in the crystal lattice dimensions of *n*ATMP·Br must be expected due to differences in alkyl chain length.

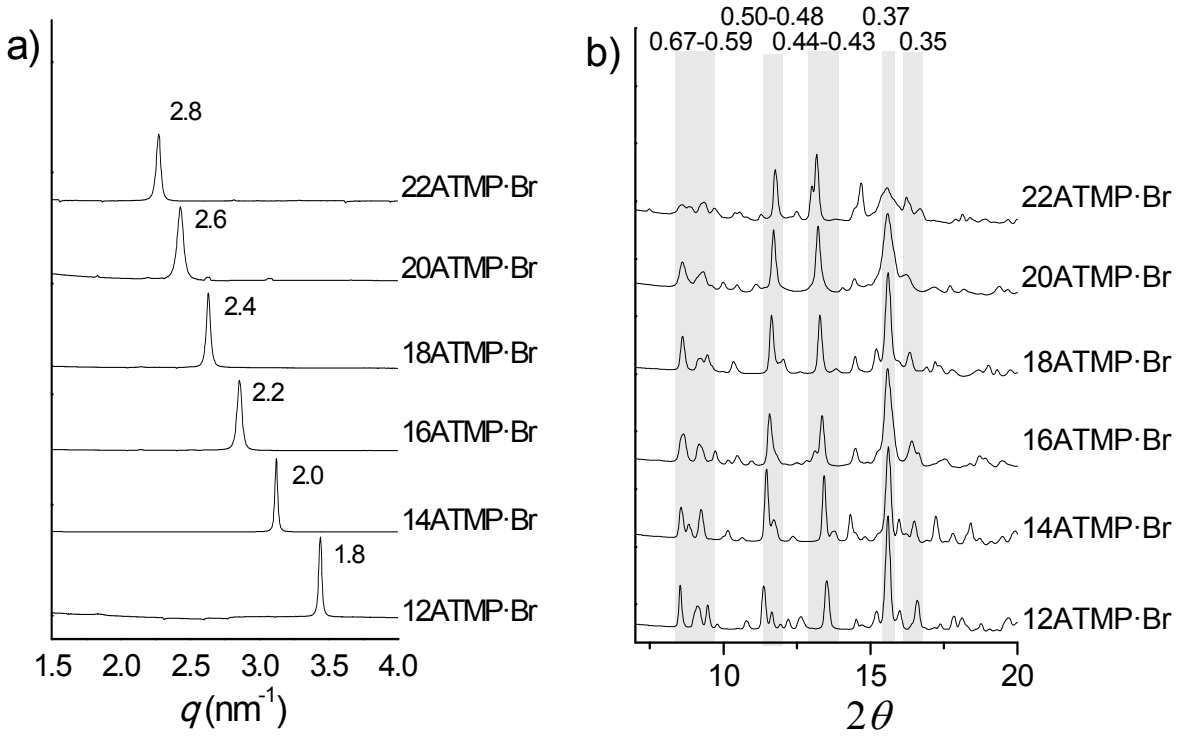

Fig. 5. Compared powder X-ray diffraction profiles of *n*ATMP·Br recorded at 25 ºC. a) SAXS region showing the sharp reflections that arise from the periodical spacing characteristic of the layered structure. b) WAXS region with shaded stripes embracing the 2θ intervals that show similar scattering. In both plots, spacings are indicated in nm.

Upon precipitation from organic solution *n*ATMP·Br rendered a microcrystalline powder with diffracting properties characteristic of Ph-I. In order to resolve the structure of this phase, a monocrystal suitable for single-crystal XRD analysis was grown from 12ATMP·Br using the vapor-diffusion method in complete absence of humidity. A picture of the analyzed crystal

together with a full account of the crystallographic data collected and handled in this study is given in the ESI file. 12ATMP·Br crystallized in a monoclinic lattice belonging to $P2_1/c$ space group, with cell parameters: a = 1.829 nm, b = 0.797 nm, c = 1.267 nm, β = 93.119º, and with a single molecule in the asymmetric unit. The compound crystallized without any solvent molecule included. An ORTEP representation of the 12ATMP·Br molecule in the conformation adopted in the crystal as well as lists of its atomic coordinates and torsion angles are given in the ESI file. The alkyl chain is in fully extended conformation and the phosphonium group deviates slightly from the average atomic plane defined for the chain. The same molecular arrangement has been found for the crystal structure of dodecylammonium bromide.[34]

A representation of the crystal structure of 12ATMP·Br as viewed along the *b*-axis is depicted in Fig. 6. The alkyl chain is oriented approximately parallel to the *ac* diagonal and molecules are packed in a biphasic array of alternating hydrophilic and hydrophobic layers. The hydrophilic layer is constituted by the trimethylphosphonium bromide groups and is approximately parallel to the *bc* plane of the crystal. Conversely, the hydrophobic domain contains the dodecyl chains, which are tilted about 30º to the plane defined by the phosphonium bromide ionic pairs. A similar conformation and packing was found for hexadecyltrimethylammonium bromide[35] although it should be mentioned that there are other reported cases in which the long alkyl chain is not fully extended.[36,37] In this structure the bromide ion is surrounded by five surfactant molecules but interacts with only one phosphonium atom which is separated by a distance of 0.413 nm. Such a distance is in agreement with that found in the trimethyl-2-phenylethylphosphonium bromide crystal (0.415 nm)[38] but significantly shorter than that reported for tetra-decylphosphonium bromide (0.486 nm).[39]

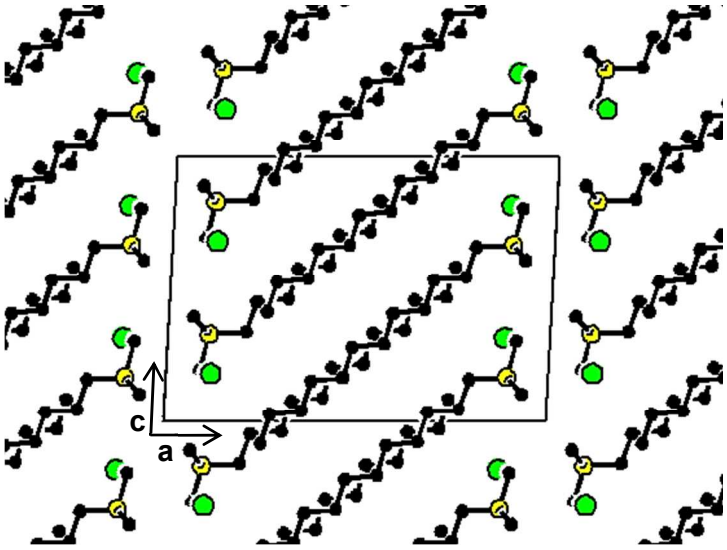

Fig. 6. View of the 12ATMP·Br crystal (Ph-I) projected along the *b*-axis with the unit cell outlined. Code colors: bromide in green, phosphorous in yellow, carbon in black; hydrogens have been omitted for clarity. (Drawn made with CERIUS^2 4.9 program, Accelrys Inc.[40]).

In Fig. 7 the powder XRD pattern simulated for a crystal lattice of 12ATMP·Br by means of the CERIUS^2 4.9 program (Accelrys Inc)[40] is compared to the pattern experimentally recorded from a powder sample of this surfactant obtained by precipitation from toluene. The crystal lattice used for simulation was modelled on the basis of the crystal unit cell determined by single crystal analysis. The extremely high coincidence attained between simulated and experimental profiles, including both SAXS and WAXS regions, leads to ascertain without ambiguity that the crystal structure adopted by 12ATMP·Br at room temperature (Ph-I) must be the same as that found in the monocrystal prepared by diffusion-evaporation.

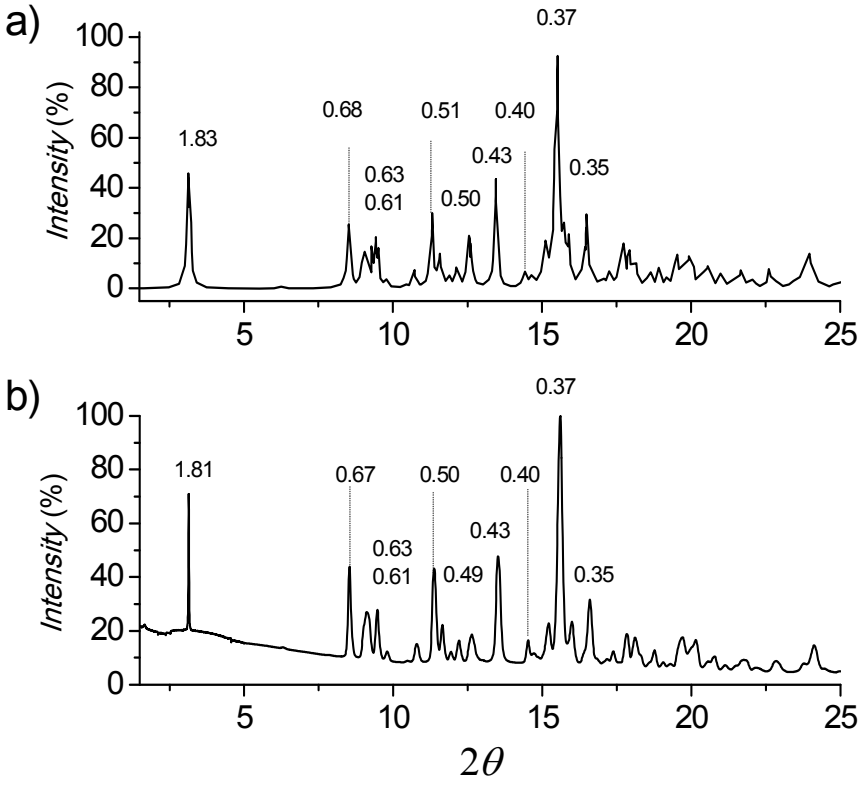

Fig. 7. Compared powder X-ray diffraction profiles of 12ATMP·Br in Ph-I. a) Profile simulated for the monoclinic crystal lattice found in the monocrystal. b) Profile experimentally obtained from the powder sample obtained by precipitation.

Respective crystal lattices were then modelled for all the other members of the *n*ATMP·Br series by taking the 12ATMP·Br monoclinic crystal structure as starting point. The methylene units necessary to enlarge properly the alkyl chain were added and the unit cell size was accordingly readjusted by changing both *a* and β parameters whereas keeping *b* and *c* at the same value as they have in 12ATMP·Br. The XRD powder profiles obtained by simulation from the crystal lattices built for *n*ATMP·Br for *n* = 14 to 22 showed again an extreme similarity with those experimentally recorded from their respective powder samples, which allowed us to conclude that the monoclinic crystal structure determined for 12ATMP·Br can be successfully extrapolated to the whole series. The unit cell parameters resulting for each *n*ATMP·Br

surfactant are provided in the ESI file, and a comparison of the most characteristic XRD spacings calculated for such unit cells with those experimentally observed is provided in Table 3.

Thermotropic behavior of *n*ATMP·Br (Phases II, III and Is)

The thermal transitions between the *n*ATMP·Br phases that were identified by DSC were then examined by XRD with synchrotron radiation. For this purpose, simultaneous SAXS and WAXS spectra were recorded at real time from each surfactant subjected to heating/cooling at a rate of 10 ºC·min^{-1} within the 10-300 ºC range. The heating traces registered every 5 ºC increasing interval are shown in Fig. 8 for 14ATMP·Br and 20ATMP·Br surfactants. In both cases clear changes were observed at the two scattering regions in agreement with the heat exchange peaks present in their respective DSC traces. In the SAXS region of 14ATMP·Br, the initial peak initially appearing at 2.0 nm jumped to 2.7 nm and it increased in intensity when the temperature reached ~75 ºC. Simultaneously, the multiple-peak scattering observed at room temperature at the WAXS region was reduced to three small groups of peaks centered at around 0.62, 0.36 and 0.31 nm. This patterns can be made to correspond to a two-dimensional pseudo-hexagonal array of a = 0.72 nm that characterizes Ph-II. A similar behavior was observed for 20ATMP·Br with the transition temperature being ~90 ºC in agreement with DSC results, and the long spacing peak jumping in this case from 2.6 nm to 3.5 nm. Nevertheless the SAXS response given by 14ATMP·Br and 20ATMP·Br to heating in the high temperature region, *i.e.* above 200 ºC, was different. In the former case, the 2.7 nm peak disappeared at ~220 ºC, whereas in the latter, the 3.5 nm peak remained practically unchanged in intensity and slightly shifted to a spacing of 3.6 nm to eventually disappears when temperature was around to 265 ºC. Such differences bring into evidence the occurrence of an additional thermotropic phase (Ph-III) previous to isotropization (Ph-Is) in 20ATMP·Br, and are consistent with the small endothermal peak that is detected in the DSC trace of this compound but that is absent in the

case of 14ATMP·Br. Comparable results were attained in the thermal XRD analysis of the others *n*ATMP·Br with 12ATMP·Br following the diffraction pattern observed for 14ATMP·Br and the remaining ones displaying a behavior similar to 20ATMP·Br (available in the ESI file). The XRD spacings collected for the full *n*ATMP·Br series along the whole range of temperatures within which they have been examined are listed for every phase in Table 3 with indication of their corresponding Miller indexes and peak intensities. These results definitively confirm the occurrence of the four phases evidenced by DSC with the existence domains such are depicted in Fig. 4.

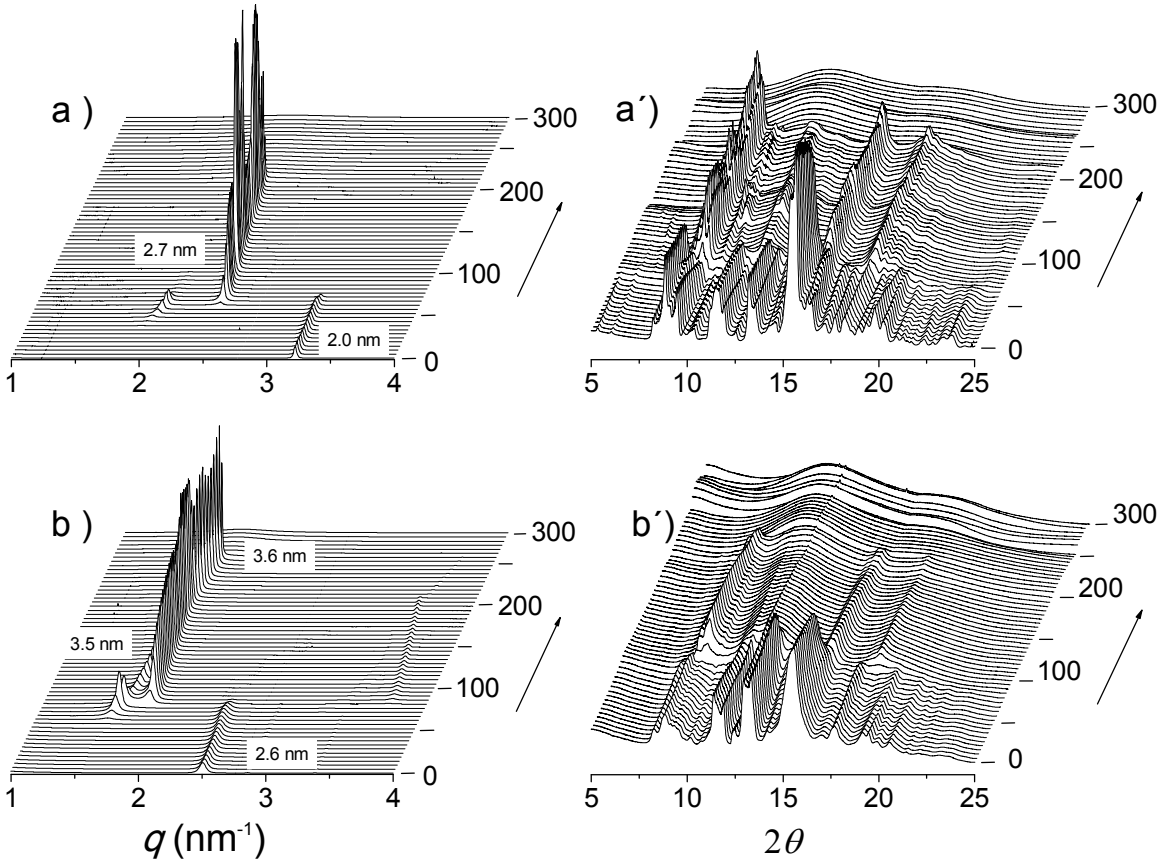

Fig 8. SAXS (left) and WAXS (right) plots from 14ATMP·Br (a,a') and 20ATMP·Br (b,b') registered at heating over the 0-300 ºC interval.

It should be noticed that thermally driven phase-interconversion in *n*ATMP·Br is not a very fast process, in particular when it takes place at relatively low temperatures. The reversibility of the Ph-I↔Ph-II↔Ph-III↔Ph-Is interconversional sequence has been examined by thermal XRD at real time by applying heating/cooling cycles at rates between 5 and 0.5 ºC·min^{-1}. It was observed that Ph-III and Ph-II were almost instantaneously recovered upon cooling from Ph-Is and Ph-III (or Ph-Is for *n* = 12 and 14) respectively, but the conversion of Ph-II into Ph-I was found to be incomplete within the applied time scale. However Ph-I could be fully recovered from Ph-II after several hours of standing at room temperature. The complete collection of XRD plots including both SAXS and WAXS profiles registered during heating/cooling cycles for the whole series is available in the ESI file.

Table 3. Observed and calculated *d*-spacings for the I, II and III phases of *n*ATMP·Br.[a]

n	**12**		**14**		**16**		**18**		**20**		**22**	
						Phase I						
	Obs.	Calc.	Obs.	Calc.	Obs.	Calc.	Obs.	Calc.	Obs.	Calc.	Obs.	Calc.
[b] *L*	1.8	1.8	2.0	2.0	2.2	2.2	2.4	2.4	2.6	2.6	2.8	2.8
hkl												
002	0.63m	0.63 (9)	0.63w	0.63 (5)	n.o	0.62 (3)	0.62m	0.62 (3)	n.o	-	n.o	-
011	0.67m	0.67 (32)	0.67m	0.67 (22)	0.67m	0.67 (21)	0.67m	0.67 (29)	0.67m	0.67 (13)	0.67m	0.66 (11)
012	0.50m	0.50 (15)	0.50m	0.49 (14)	0.50m	0.49 (12)	0.49m	0.49 (8)	0.49s	0.48 (7)	0.49s	0.48 (5)
013	0.37s	0.37 (22)	0.37s	0.37 (18)	0.37s	0.37 (17)	0.37s	0.37 (12)	0.37s	0.37 (9)	0.37s	0.37 (7)
121		0.37 (100)		0.37 (100)		0.37 (100)		0.37 (100)		0.37 (100)		0.37 (100)
020	0.40w	0.40 (9)	0.40m	0.40 (4)	0.40m	0.40 (15)	0.40m	-	0.40m	0.40 (10)	0.40m	0.40 (11)
$10\bar{2}$	0.61m	0.61 (10)	0.62m	0.62 (12)	0.63m	0.63 (10)	0.63m	0.64 (7)	0.63m	0.63 (4)	0.62m	0.63 (3)
221	0.35m	0.35 (34)	0.35m	0.35 (29)	0.35m	0.35 (23)	0.35m	0.35 (22)	0.35m	0.36 (18)	0.35m	0.36 (17)
302	0.43m	0.43 (53)	0.43m	0.44 (55)	0.43m	0.44 (51)	0.43m	0.44 (52)	0.44s	0.44 (44)	0.44s	0.45 (45)
						Phase II						
L	2.4		2.7		2.9		3.2		3.5		3.7	
hkl												
010	0.63-0.62		0.64-0.60		0.62-0.60		0.65-0.62		0.64-0.62		0.64-0.62	
011	0.36		0.36		0.36		0.36		0.36		0.36	
020	0.31		0.31		0.31		0.31		0.31		0.31	
						Phase III						
L	-		-		3.0		3.3		3.6		3.8	

[a] The intensity of peaks (in parenthesis) are visually estimated for observed reflections and given in normalized % for calculated reflexions. [b] *L* is referred to the 100 spacing.

The textures of the phases characterized for *n*ATMP·Br were evidenced by polarizing optical microscopy observation carried out on heated/cooled samples along the same temperature ranges than used for DSC and XRD analysis. Representative optical micrographs of the three phases adopted by 14ATMP·Br are shown in Fig. 9. Pictures were taken from the same area of the surfactant film (initially Ph-I), which was first heated to 250 ºC for isotropization (Ph-Is) and then slowly cooled down to room temperature to recover Ph-I by passing through Ph-II. The observed differences in texture for Ph-I before and after treatment are reasonable due to differences in thermal history and also to a probably incomplete conversion of Ph-II. The texture displayed by Ph-II at 150 ºC is indicative of a smectic arrangement although no so clearly as to be able to identify the smectic phase that is dealing with.

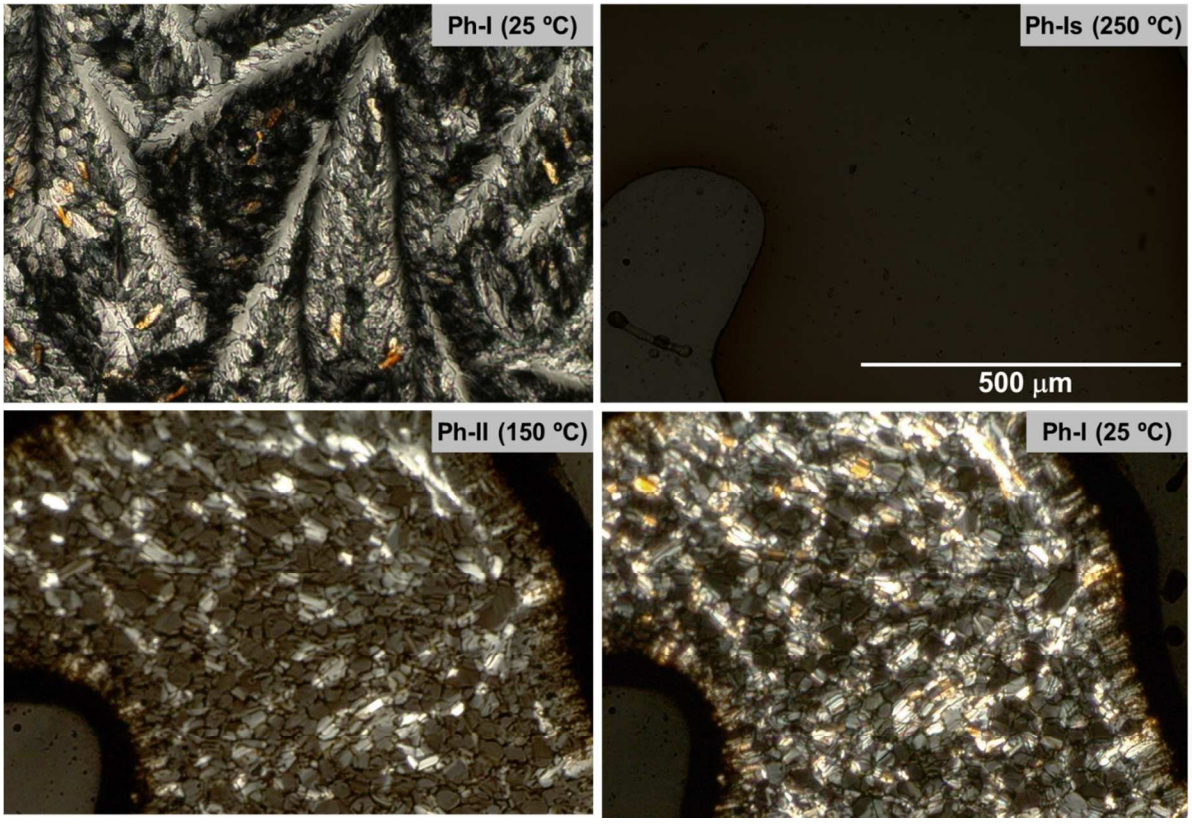

Fig. 9. POM micrographs of 14ATMP·Br recorded at the indicated temperatures.

The POM pictures recorded from 20ATMP·Br following a similar protocol are depicted in Fig.10. In this case the four phases previously identified for this compound by DSC and XRD were clearly brought into evidence. The initial microcrystalline powder of Ph-I that is observed at room temperature was first isotropicized at 300 ºC (Ph-Is). Upon cooling at 230 ºC the isotropic phase converted into Ph-III displaying a focal-conic fan-like texture characteristic of a Smectic-A structure. Upon further cooling to 190 ºC, the morphology slightly changed to show a more polygonal texture lacking fan shapes but consistent with the occurrence of a Smectic-B phase (Ph-II). A careful inspection of the pictures recorded along the whole Ph-II domain of temperatures, reveals for this phase the presence of frequent non-regular striations that intensify as temperature decreases. The Ph-I recovered by cooling at 30 ºC displays conspicuous black stripes reminiscent of the striations present in Ph-II. This is a very interesting observation that brings out the close structural interrelation between the semicrystalline Ph-II and the full crystalline Ph-I. A complete assortment of POM pictures illustrating the phase textures for the whole series of *n*ATMP·Br is included in the ESI file.

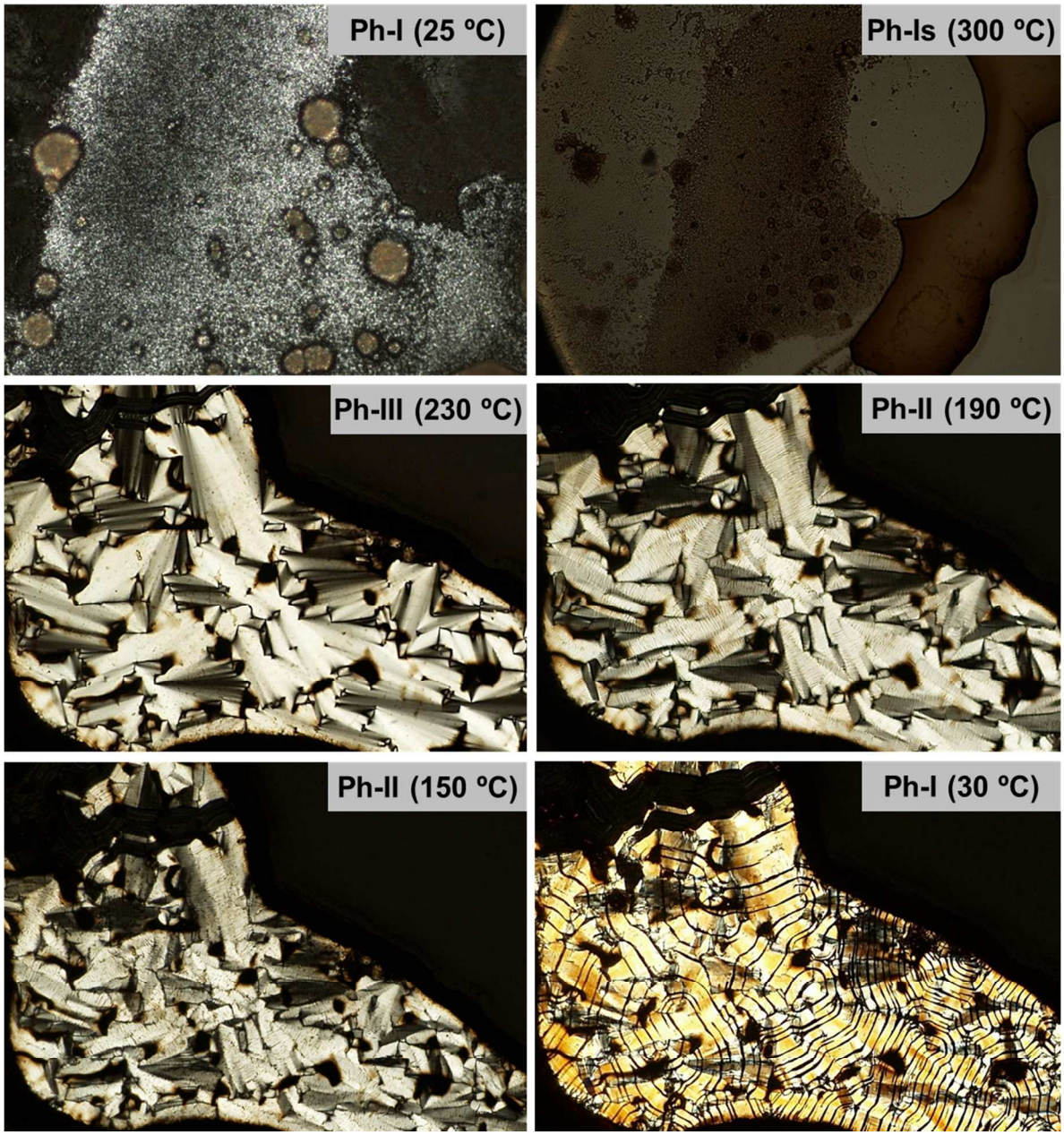

Fig. 10. POM micrographs of 20ATMP·Br recorded at the indicated temperatures.

The molecular arrangements in the *n*ATMP·Br phases

The *L* values for the *n*ATMP·Br phases displaying long-range order are plotted against *n* in Fig. 11. A remarkable feature of this plot is that an almost straight linear fitting is observed for every phase and that lines with very similar equations in both gradient and *L*-intercept are displayed for the phases formed upon heating (Ph-II and Ph-III). On the other hand, the *L*-*n* points for Ph-I become almost perfectly aligned along a straight line that is significantly displaced downwards and has a slightly smaller slope. The graphical analysis of the *L*-*n* plots reveals relevant details of the phase geometry as they are the thickness of both the polar layer containing the trimethylphosphonium-bromide pairs (L_0) and the paraffinic layer containing the long alkyl chains (L-L_0). The ratio of L-L_0 to the length of the alkyl chain in *all-trans* conformation (l) gives indication of the shortening undergone by the structure due to chain tilting, degree of interpenetration or occurrence of *gauche* conformation effects. The results of these calculations are compared in Table 4.

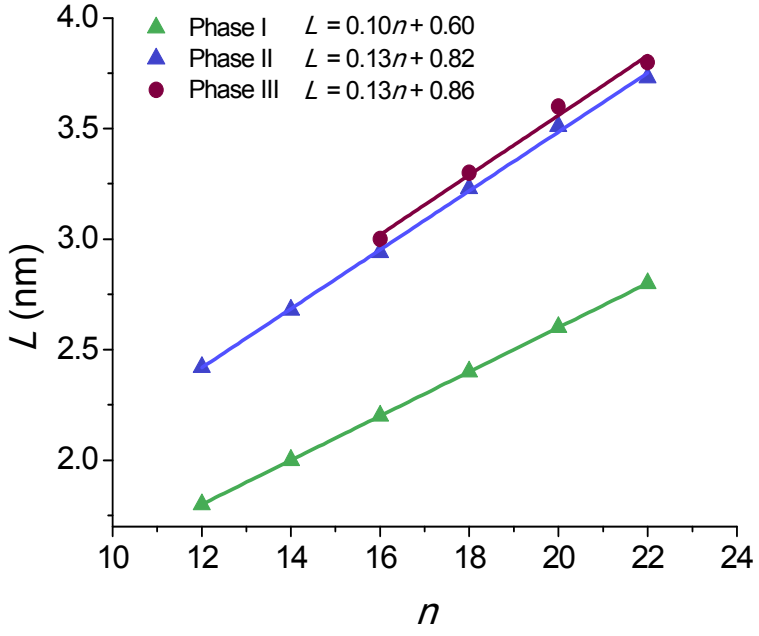

Fig.11. Plot of the long spacing *L* measured by SAXS against *n* for the crystalline and liquid-crystal phases found in *n*ATMP·Br.

The *L*-*n* straight line for Ph-I has a slope of 0.1 nm/CH_2 and an *L*-intercept of 0.6 nm. The shrinkage ratio of the paraffinic layer is pretty constant along the series with a value of 0.80. These data are in full agreement with the molecular arrangement put forward for the crystal structure of these compounds on the basis of the monocrystal XRD analysis of 12ATMP·Br, i.e. the alkyl chains are crystallized in a almost fully interdigitated arrangement and are tilted about 37º respects to the basal plane of the structure. Furthermore the ionic layer thickness of 0.6 nm defined by the *L*-intercept is also consistent with the molecular volume calculated for the trimethylphosphonium-bromide pair as it is arranged in the crystal.

Table 4. Geometrical parameters for the *n*ATMP·Br phases.

		Phase I			Phase II			Phase III		
n	l^a	L^b	L_o^c	$(L-L_0)/l$	L	L_o	$(L-L_0)/l$	L	L_o	$(L-L_0)/l$
12	1.5	1.8	0.6	0.80	2.4	0.82	1.06		-	-
14	1.75	2.0	0.6	0.80	2.7	0.82	1.06	-	-	-
16	2.0	2.2	0.6	0.80	2.9	0.82	1.06	3.0	0.86	1.06
18	2.25	2.4	0.6	0.80	3.2	0.82	1.06	3.3	0.86	1.06
20	2.5	2.6	0.6	0.80	3.5	0.82	1.06	3.6	0.86	1.06
22	2.75	2.8	0.6	0.80	3.7	0.82	1.06	3.8	0.86	1.06

[a]Length of the alkyl chain in fully extended conformation. [b]Interplanar spacing experimentally observed by SAXS. [c]Thickness of the Me_3P^+ Br^- ionic-pair layer.

The geometrical parameters resulting from the analysis of the Ph-II plot are clearly different from those calculated for Ph-I. The large expansion in *L* taking place when Ph-I converts into Ph-II entails a considerable enlargement of L_0 in spite that line slope becomes now about 0.13 nm/CH_2. Also the $(L-L_0)/l$ ratio is larger for Ph-II than for Ph-I attaining now a value close to unity. These values are in agreement with a layered structure in which the alkyl chains are still fully or almost fully interdigitated and standing approximately normal to the basal plane of the structure. The larger thickness displayed by the polar layer can be explained by assuming that a rearrangement has occurred in the packing of the ion pairs within this layer. According to

data provided by XRD it is reasonable to interpret therefore that Ph-II consists of a "semicrystalline" phase (Smectic-B) in which the polar heads of the surfactant remain crystallized in a pseudo-hexagonal array whereas the alkyl tails with a quasi-extended conformation are side-by-side packed without crystalline order.

Ph-III is only observed for *n*ATMP·Br with $n \geq 16$. The graphical differences found between *L*-*n* plots of Ph-II and Ph-III are non-relevant and only entail a small expansion (less than ~5%) in both *L* and L_0. However the scattering produced by Ph-III in the WAXS region merely consists of a broad plateau centered on ~0.5 nm without showing any vestige of discrete scattering characteristic of crystalline material. The structure of this phase is therefore envisaged as a Smetic-A phase in which the trimethylphosphonium bromides continue to be confined in layers but without crystalline order and the alkyl chains are filling the interlayer paraffinic space in an arrangement close to that adopted in Ph-II.

A simple scheme sketching approximately the molecular arrangements adopted in Ph-I, Ph-II and Ph-III of *n*ATMP·Br is depicted in Fig.12. Accordingly the description of the thermal phase conversion process can be envisaged as follows: The I/II transition involves melting/crystallization of the paraffinic layer together with a slight rearrangement of the phosphonium-bromide pairs, that converts the monoclinic lattice present in Ph-I into the two-dimensional pseudo-hexagonal array present in Ph-II and vice versa. The transition from Ph-II to Ph-III implies the complete melting of the ionic layer and probably an increased disordering of the paraffinic core although the polymethylene chains must remain essentially extended to maintain the long periodicity revealed by SAXS. Finally a complete disordering takes places when Ph-III is converted in the isotropic phase Ph-Is. The direct conversion of Ph-II into Ph-Is that is observed for 12ATMP·Br and 14ATMP·Br is thought to be due to the incapacity of these compounds to generate a stable Ph-III because the insufficient length that the polymethylene chain has in these cases.

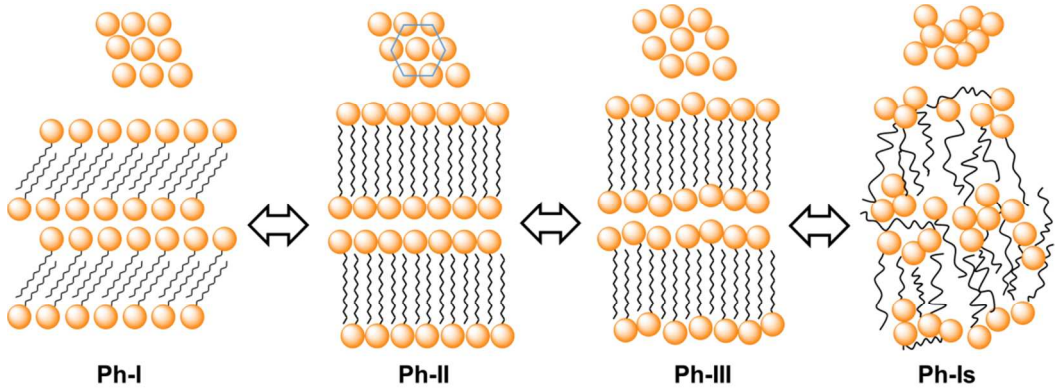

Fig. 12. Scheme of the molecular arrangements adopted in the *n*ATMP·Br phases. On the top the 2D array of the polar heads in the 100 planes are depicted indicating that it changes from oblique in Ph-I to pseudo-hexagonal in Ph-II to become finally disordered, in Ph-III. In Ph-Is the 2D arrangement is lost.

Conclusions

A series of alkyltrimethylphosphonium bromides (*n*ATMP·Br) bearing linear alkyl chains of even numbers (*n*) of carbon atoms from 12 to 22 has been synthesized and chemically characterized. These amphiphilic compounds have Krafft temperatures steadily going up from below 0 up to 55 ºC for increasing values of *n*, and they show *cmc* values lower than those reported for their alkyltrimethylammonium bromides analogs. *n*ATMP·Br appear to be high thermally stable compounds with onset decomposition temperatures close to 400 ºC. Their response to heating within the 0-300 ºC range of temperatures involves two or three thermotropic transitions depending on *n*. At room temperature, all *n*ATMP·Br crystallize in a monoclinic lattice with the Me_3P·Br ionic heads arranged in layers and the long alkyl chains in fully extended conformation, filling the interlayer spacing with a tilted orientation. This crystalline phase is converted upon heating into a Smectic-B phase that maintains a similar stratified arrangement but with the alkyl chains in the molten state. For $n \geq 16$, the Smectic-B phase changes to Smectic-A when heated around 225 ºC to become finally isotropic when

temperatures rise above 240 ºC. For *n* = 12 and 14, isotropization occurs at 215-220 ºC without formation of the Smectic-A phase. All the thermal transitions observed for *n*ATMP·Br are reversible but proceed at moderate rates in particular when they take place at low temperatures.

Acknowledgements

This work received financial support from MCINN (Spain) with Grant MAT2012-38044-C03. Portions of this research were carried out at the BL11 line of ALBA synchrotron (Cerdanyola, Spain) with the invaluable support of Dr. Christina Kamma-Lorger. Authors are indebted to Dr. Luis Oriol (Universidad de Zaragoza) for useful comments on the structure of the liquid crystal phases. Thanks also to the MICINN for the Ph.D. grant awarded to Ana Gamarra.

References

1 W. Xie, R. Xie, W. P. Pan, D. Hunter, B. Koene, L. S. Tan and R. Vaia, *Chem. Mater.*, 2002, **14**, 4837–4845.

2 K. J. Fraser, R. Douglas and MacFarlane, *Aust. J. Chem.*, 2009, **62**, 309–321.

3 D. A. Gerritsma, A. Robertson, J. McNulty and A. Capretta, *Tetrahedron Lett.*, 2004, **45**, 7629–7631.

4 N. Ito, S. Arzhantsev, M. Heitz and M. Maroncelli, *J. Phys. Chem. B*, 2004, **108**, 5771–5777.

5 J. McNulty, A. Capretta, J. Wilson, J. Dyck, G. Adjabeng and A. Robertson, *Chem. Commun. (Camb).*, 2002, 1986–1987.

6 T. Ramnial, D. D. Ino and J. A. C. Clyburne, *Chem. Commun. (Camb).*, 2005, 325–327.

7 G. Panek, S. Schleidt, Q. Mao, M. Wolkenhauer, H. W. Spiess and G. Jeschke, *Macromolecules*, 2006, **39**, 2191–2200.

8 C. B. Hedley, G. Yuan and B. K. G. Theng, *Appl. Clay Sci.*, 2007, **35**, 180–188.

9 C. Byrne and T. McNally, *Macromol. Rapid Commun.*, 2007, **28**, 780–784.

10 A. Cieniecka-Rosłonkiewicz, J. Pernak, J. Kubis-Feder, A. Ramani, A. J. Robertson and K. R. Seddon, *Green Chem.*, 2005, **7**, 855–862.

11 V. Kumar and S. V Malhotra, *Bioorg. Med. Chem. Lett.*, 2009, **19**, 4643–4646.

12 K. Binnemans, *Chem. Rev.*, 2005, **105**, 4148–4204.

13 K. V. Axenov and S. Laschat, *Materials (Basel).*, 2011, **4**, 206–259.

14 S. Kamitori, Y. Sumimoto, K. Vongbupnimit, K. Noguchi and K. Okuyama, *Mol. Cryst. Liq. Cryst.*, 1997, **300**, 31–43.

15 A. Kanazawa, O. Tsutsumi, T. Ikeda and Y. Nagase, *J. Am. Chem. Soc.*, 1997, **119**, 7670–7675.

16 G. Adamová, R. L. Gardas, L. P. N. Rebelo, A. J. Robertson and K. R. Seddon, *Dalt. Trans.*, 2011, **40**, 12750–12764.

17 D. J. Abdallah, A. Robertson, H. Hsu and R. G. Weiss, *J. Am. Chem. Soc.*, 2000, **122**, 3053–3062.

18 D. J. Abdallah, R. E. Bachman, J. Perlstein and R. G. Weiss, *J. Phys. Chem. B*, 1999, **103**, 9269–9278.

19 A. Kanazawa, T. Ikeda and T. Endo, *Antimicrob. Agents Chemother.*, 1994, **38**, 945–952.

20 M. Antonietti, J. Conrad and A. Thuenemann, *Macromolecules*, 1994, **27**, 6007–6011.

21 G. Pérez-Camero, M. García-Álvarez, A. M. de Ilarduya, C. Fernández, L. Campos and S. Muñoz-Guerra, *Biomacromolecules*, 2004, **5**, 144–152.

22 A. Tolentino, A. Alla, A. Martínez de Ilarduya and S. Muñoz-Guerra, *Carbohydr. Polym.*, 2011, **86**, 484–490.

23 A. Tolentino, A. Alla, A. M. De Ilarduya and S. Muñoz-Guerra, *Carbohydr. Polym.*, 2013, **92**, 691–696.

24 A. Tolentino, A. Alla, A. Martínez de Ilarduya and S. Muñoz-Guerra, *Int. J. Biol. Macromol.*, 2014, **66**, 346–353.

25 A. Tolentino, A. Alla and S. Muñoz-Guerra, *Eur. Polym. J.*, 2012, **48**, 1838–1845.

26 Y. S. Lee and K. W. Woo, *J. Colloid Interface Sci.*, 1995, **169**, 34–38.

27 A. Tolentino, A. Alla, A. Martinez de Ilarduya, M. Font-Bardia, S. Leon and S. Munoz-Guerra, *RSC Adv.*, 2014, **4**, 10738–10750.

28 G. M. Sheldrick, *Acta Crystallogr.*, 2015, **C71**, 3-8.

29 G. Witschard and C. E. Griffin, *Spectrochim. Acta*, 1963, **19**, 1905–1910.

30 M. Arshad A. Beg and Samiuzzaman, *Tetrahedron*, 1968, **24**, 191–198.

31 T. W. Davey, W. a Ducker, A. R. Hayman and J. Simpson, *Langmuir*, 1998, **14**, 3210–3213.

32 H. a. Patel, R. S. Somani, H. C. Bajaj and R. V. Jasra, *Appl. Clay Sci.*, 2007, **35**, 194–200.

33 K. Iwamoto, Y. Ohnuki, K. Sawada and M. Seno, *Mol. Cryst. Liq. Cryst.*, 1981, **73**, 95–103.

34 B.-M. Lundén, *Acta Crystallogr.*, 1974, **B30**, 1756–1760.

35 A. R. Campanelli and L. Scaramuzza, *Acta Crystallogr. Sect. C*, 1986, **C42**, 1380–1383.

36 V. Ermolaev, V. Miluykov, I. Rizvanov, D. Krivolapov, E. Zvereva, S. Katsyuba, O. Sinyashin and R. Schmutzler, *Dalt. Trans.*, 2010, **39**, 5564–5571.

37 C. M. Wang, T. Y. Chang, C. W. Chiu, H. M. Lin and K. H. Lii, *Inorg. Chem.*, 2014, **53**, 3266–3268.

38 F. G. Riddell, M. Rogerson, W. B. Turnbull and F. Fülöp, *J. Chem. Soc. Perkin Trans. 2*, 1997, 95–100.

39 D. J. Abdallah, R. E. Bachman, J. Perlstein and R. G. Weiss, *J. Phys. Chem. B*, 1999, **103**, 9269–9278.

40 Accelrys Cerius^2 Manual, *4.9 ed., Accelrys Inc., 2003.*

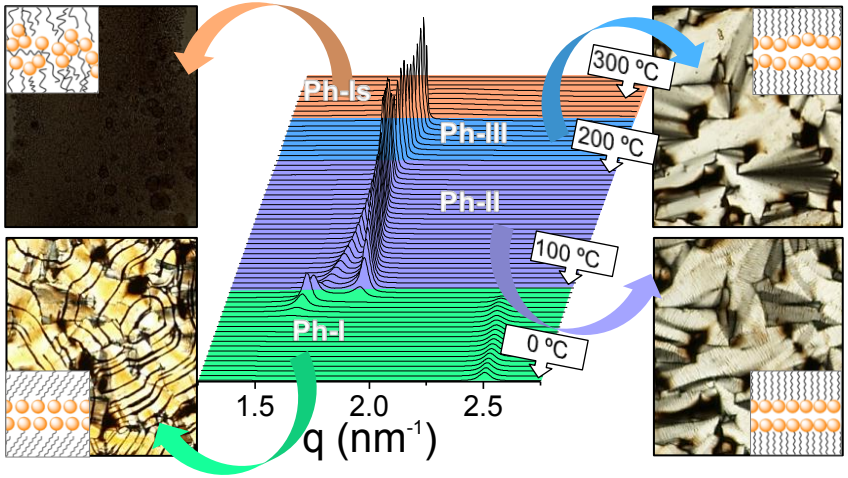
Ph-Is
Ph-III
Ph-II
Ph-I
300 °C
200 °C
100 °C
0 °C
1.5
2.0
2.5
q (nm-1)

Electronic Supplementary Information

Crystalline Structure and Thermotropic Behavior of Alkyltrimethylphosphonium Amphiphiles

Ana Gamarra, Lourdes Urpí, Antxon Martínez de Ilarduya and Sebastián Muñoz-Guerra*

Departament d'Enginyeria Química, Universitat Politècnica de Catalunya, ETSEIB, Diagonal 647, Barcelona 08028, Spain.

E-mail: sebastian.munoz@upc.edu

Contents

Experimental procedures

Figures

Fig. SI-9. SAXS (left) and WAXS (right) plots from 14ATMP·Br registered over the 0-300 ºC interval. a) heating, b) slow cooling, c) fast cooling and d) reheating.

Fig. SI-10. SAXS (left) and WAXS (right) plots from 16ATMP·Br registered over the 10-280 ºC interval. a) heating, b) cooling and c) reheating.

Fig. SI-11. SAXS (left) and WAXS (right) plots from 18ATMP·Br registered over the 10-280 ºC interval. a) heating, b) cooling and c) reheating.

Fig. SI-12. SAXS (left) and WAXS (right) plots from 20ATMP·Br registered over the 0-300 ºC interval. a) heating, b) slow cooling, c) fast cooling and d) reheating.

Fig. SI-13. SAXS (left) and WAXS (right) plots from 22ATMP·Br registered over the 10-280 ºC interval. a) heating, b) cooling and c) reheating.

Fig. SI-14. Graphical comparison of the observed (at 25 ºC) and calculated main *d*-spacings (nm) with $h \neq 0$ for *n*ATMP·Br.

Fig. SI-15. POM micrographs recorded from *n*ATMP·Br at the indicated temperatures.

Tables

Table SI-1. Crystal data and structure refinement for 12ATMP·Br.

Table SI-2. Atomic coordinates (x 10^4) and equivalent isotropic displacement parameters ($Å^2$ x 10^3) for 12ATMP·Br. U (eq) is defined as one third of the trace of the orthogonalized Uij tensor.

Table SI-3. Bond lengths (Å) and angles (º) for 12ATMP·Br.

Table SI-4. Anisotropic displacement parameters ($Å^2$ x 10^3) for 12ATMP·Br. The anisotropic displacement factor exponent takes the form: $-2\pi^2 [h^2 a^{*2} U_{11} + ... + 2 h k a^* b^* U_{12}]$.

Table SI-5. Torsion angles (º) for 12ATMP·Br.

Table SI-6. Crystallographic *a* and β values of the *n*ATMP·Br salts used for modelling and the crystal lattices from which SAXS and WAXS profiles were simulated.

Contents

Experimental procedures

1. General procedure for the synthesis of trimethylalkylphosphonium salts (*n*ATMP·Br)

1-bromoalkane (5.5 mmol) was placed in a flask immersed into an oil bath (80 ºC) and under a nitrogen atmosphere. After heating for several minutes, the trimethylphosphine (TMP) was slowly added (5 mL, 5 mmol). The mixture was heated up to 116 ºC and stirred for a period of 18 to 24 h depending on the bromoalkane used. The precipitate that appeared upon cooling to room temperature, was collected by filtration, washed several times to remove the excess of alkylbromide, and finally dried under high vacuum.

Dodecyltrimethylphosphonium bromide (12ATMP·Br)

TMP and 1.3 mL of 1-bromododecane gave after 16 h stirring 1.14 g (70%) of the product as a white powder. The chemical structure was ascertained by ^{1}H NMR, ^{13}C NMR, FT-IR and elemental analysis. ^{1} H NMR (300.1 MHz; $CDCl_3$; δ(ppm)): 2.46 (2H, m, RC**H**$_2$P$^+$), 2.25 and 2.20 (9H, d, P$^+$(C**H**$_3$)$_3$), 1.55 (4H, m, RC**H**$_2$C**H**$_2$CH$_2$P$^+$), 1.25 (16H, m, CH$_3$-(C**H**$_2$)$_8$-CH$_2$ CH$_2$P$^+$), 0.88 (3H, t, C**H**$_3$-(CH$_2$)$_{11}$-P$^+$), ^{13} C NMR (75.5 MHz; $CDCl_3$; δ(ppm)): 31.9 (CH$_3$-CH$_2$-**C**H$_2$R), 30.6 (CH$_3$-CH$_2$-CH$_2$-**C**H$_2$R), 30.4-29.0 (CH$_3$-CH$_2$-CH$_2$-(**C**H$_2$)$_5$R), 24.1 (R**C**H$_2$CH$_2$CH$_2$P$^+$), 23.4 (R**C**H$_2$P$^+$), 22.6 (CH$_3$- **C**H$_2$R), 21.8 (R**C**H$_2$-CH$_2$-P$^+$), 14.1 (**C**H$_3$R), 9.4 and 8.6 (P$^+$(**C**H$_3$)$_3$). FT-IR (ν(cm^{-1})): 2913, 2847, 1471, 972, 705. Elemental analysis: C (%): 55.53; found: 55.53, H (%): 10.59; found: 10.50.

Tetradecyltrimethylphosphonium bromide (14ATMP·Br)

TMP and 1.5 mL of 1-bromotetradecane gave after 17 h stirring 1.43 g (80%) of the product as a white powder. The chemical structure was ascertained by ^{1}H NMR, ^{13}C NMR, FT-IR and elemental analysis. ^{1} H NMR (300.1 MHz; $CDCl_3$; δ(ppm)): 2.46 (2H, m, RC**H**$_2$P$^+$), 2.25 and 2.20 (9H, d, P$^+$(C**H**$_3$)$_3$), 1.55 (4H, m, RC**H**$_2$C**H**$_2$CH$_2$P$^+$), 1.25 (20H, m, CH$_3$-(C**H**$_2$)$_{10}$-CH$_2$ CH$_2$P$^+$), 0.88 (3H, t, C**H**$_3$-(CH$_2$)$_{13}$-P$^+$), ^{13} C NMR (75.5 MHz; $CDCl_3$; δ(ppm)): 31.9 (CH$_3$-CH$_2$-**C**H$_2$R), 30.6 (CH$_3$-CH$_2$-CH$_2$-**C**H$_2$R), 30.4-29.0 (CH$_3$-CH$_2$-CH$_2$-(**C**H$_2$)$_7$R), 24.1 (R**C**H$_2$CH$_2$CH$_2$P$^+$), 23.4 (R**C**H$_2$P$^+$), 22.6 (CH$_3$- **C**H$_2$R), 21.8 (R**C**H$_2$-CH$_2$-P$^+$), 14.1 (**C**H$_3$R), 9.4 and 8.6 (P$^+$(**C**H$_3$)$_3$). FT-IR (ν(cm^{-1})): 2911, 2856, 1469, 978, 718. Elemental analysis: C (%): 57.92; found: 58.03, H (%): 10.90; found: 10.79.

Hexadecyltrimethylphosphonium bromide (16ATMP·Br)

TMP and 1.7 mL of 1-bromohexadecane gave after 18 h stirring 1.62 g (85%) of the product as a white powder. The chemical structure was ascertained by ^{1}H NMR, ^{13}C NMR, FT-IR and elemental analysis. ^{1} H NMR (300.1 MHz; $CDCl_3$; δ(ppm)): 2.47 (2H, m, RC**H**$_2$P$^+$), 2.25 and 2.20 (9H, d, P$^+$(C**H**$_3$)$_3$), 1.55 (4H, m, RC**H**$_2$C**H**$_2$CH$_2$P$^+$), 1.25 (24H, m, CH$_3$-(C**H**$_2$)$_{12}$-CH$_2$ CH$_2$P$^+$), 0.88 (3H, t, C**H**$_3$-(CH$_2$)$_{15}$-P$^+$), ^{13} C NMR (75.5 MHz; $CDCl_3$): 31.9 (CH$_3$-CH$_2$-**C**H$_2$R), 30.6 (CH$_3$-CH$_2$-CH$_2$-**C**H$_2$R), 30.4-29.0 (CH$_3$-CH$_2$-CH$_2$-(**C**H$_2$)$_9$R), 24.1 (R**C**H$_2$CH$_2$CH$_2$P$^+$), 23.4 (R**C**H$_2$P$^+$), 22.6 (CH$_3$- **C**H$_2$R), 21.8 (R**C**H$_2$-CH$_2$-P$^+$), 14.1 (**C**H$_3$R), 9.4 and 8.6 (P$^+$(**C**H$_3$)$_3$). FT-IR (ν(cm^{-1})): 2912, 2848, 1472, 981, 716. Elemental analysis: C (%): 59.96; found: 60.06, H (%): 11.16; found: 11.00.

Octadecyltrimethylphosphonium bromide (18ATMP·Br)
TMP and 1.9 mL of 1-bromooctadecane gave after 20 h stirring 1.45 g (70%) of the product as a white powder. The chemical structure was ascertained by ^{1}H NMR, ^{13}C NMR, FT-IR and elemental analysis. ^{1} H NMR (300.1 MHz; $CDCl_3$; δ(ppm)): 2.47 (2H, m, RC**H**$_2$P$^+$), 2.25 and 2.20 (9H, d, P$^+$(C**H**$_3$)$_3$), 1.50 (4H, m, RC**H**$_2$C**H**$_2$CH$_2$P$^+$), 1.26 (28H, m, CH$_3$-(C**H**$_2$)$_{14}$-CH$_2$ CH$_2$P$^+$), 0.88 (3H, t, C**H**$_3$-(CH$_2$)$_{15}$-P$^+$), ^{13} C NMR (75.5 MHz; $CDCl_3$; δ(ppm)): 31.9 (CH$_3$-CH$_2$-**C**H$_2$R), 30.6 (CH$_3$-CH$_2$-CH$_2$-**C**H$_2$R), 30.4-29.0 (CH$_3$-CH$_2$-CH$_2$-(**C**H$_2$)$_{11}$R), 24.1 (R**C**H$_2$CH$_2$CH$_2$P$^+$), 23.4 (R**C**H$_2$P$^+$), 22.6 (CH$_3$- **C**H$_2$R), 21.8 (R**C**H$_2$-CH$_2$-P$^+$), 14.1 (**C**H$_3$R), 9.4 and 8.6 (P$^+$(**C**H$_3$)$_3$). FT-IR (ν(cm^{-1})) : 2915, 2849, 1472, 991, 714. Elemental analysis: C (%): 61.73; found: 61.56, H (%): 11.38; found: 11.22.

Eicosyltrimethylphosphonium bromide (20ATMP·Br)
TMP and 2.0 g of 1-bromoeicosane gave after 22 h stirring 1.7 g (80%) of the product as a white powder. The chemical structure was ascertained by ^{1}H NMR, ^{13}C NMR, FT-IR and elemental analysis. ^{1} H NMR (300.1 MHz; $CDCl_3$; δ(ppm)): 2.47 (2H, m, RC**H**$_2$P$^+$), 2.25 and 2.20 (9H, d, P$^+$(C**H**$_3$)$_3$), 1.50 (4H, m, RC**H**$_2$C**H**$_2$CH$_2$P$^+$), 1.26 (32H, m, CH$_3$-(C**H**$_2$)$_{16}$-CH$_2$ CH$_2$P$^+$), 0.88 (3H, t, C**H**$_3$-(CH$_2$)$_{15}$-P$^+$), ^{13} C NMR (75.5 MHz; $CDCl_3$; δ(ppm)): 31.9 (CH$_3$-CH$_2$-**C**H$_2$R), 30.6 (CH$_3$-CH$_2$-CH$_2$-**C**H$_2$R), 30.4-29.0 (CH$_3$-CH$_2$-CH$_2$-(**C**H$_2$)$_{13}$R), 24.1 (R**C**H$_2$CH$_2$CH$_2$P$^+$), 23.4 (R**C**H$_2$P$^+$), 22.6 (CH$_3$- **C**H$_2$R), 21.8 (R**C**H$_2$-CH$_2$-P$^+$), 14.1 (**C**H$_3$R), 9.4 and 8.6 (P$^+$(**C**H$_3$)$_3$). FT-IR (ν(cm^{-1})): 2915, 2848, 1478, 986, 711. Elemental analysis: C (%): 63.26; found: 63.12, H (%): 11.58; found: 11.37.

Docosyltrimethylphosphonium bromide (22ATMP·Br)
TMP and 2.1 g of 1-bromodocosane gave after 24 h stirring 1.6 g (70%) of the product as a white powder. The chemical structure was ascertained by ^{1}H NMR, ^{13}C NMR, FT-IR and elemental analysis. ^{1} H NMR (300.1 MHz; $CDCl_3$; δ(ppm)): 2.47 (2H, m, RC**H**$_2$P$^+$), 2.25 and 2.20 (9H, d, P$^+$(C**H**$_3$)$_3$), 1.50 (4H, m, R C**H**$_2$C**H**$_2$CH$_2$P$^+$), 1.26 (36H, m, CH$_3$-(C**H**$_2$)$_{18}$-CH$_2$ CH$_2$P$^+$), 0.88 (3H, t, C**H**$_3$-(CH$_2$)$_{15}$-P$^+$), ^{13} C NMR (75.5 MHz; $CDCl_3$; δ(ppm)): 31.9 (CH$_3$-CH$_2$-**C**H$_2$R), 30.6 (CH$_3$-CH$_2$-CH$_2$-**C**H$_2$R), 30.4-29.0 (CH$_3$-CH$_2$-CH$_2$-(**C**H$_2$)$_{15}$R), 24.1 (R**C**H$_2$CH$_2$CH$_2$P$^+$), 23.4 (R**C**H$_2$P$^+$), 22.6 (CH$_3$- **C**H$_2$R), 21.8 (R**C**H$_2$-CH$_2$-P$^+$), 14.1 (**C**H$_3$R), 9.4 and 8.6 (P$^+$(**C**H$_3$)$_3$). FT-IR (ν(cm^{-1})): 2911, 2848, 1474, 989, 716. Elemental analysis: C (%): 64.61; found: 64.70, H (%): 11.75; found: 11.65.

2. Methodology used for the single-crystal analysis

A crystal of 12ATMP·Br was mounted on a D8 Venture diffractometer, the radiation used was from a microfocus with a multilayer monochromator with Mo-Kα radiation (λ = 0.071073 nm), and the diffraction was collected with an area detector Photon 100 CMOS. The unit cell parameters were determined from 7111 reflections (2.23º < θ < 25.14º) and refined by least-squares method. Intensities of 25175 reflections (2.23º < θ < 25.39º) were collected, 3385 of which were unique (R_{int} = 0.0429), and 2530 unique reflections were considered as observed (conditions $I > 2\sigma(I)$). Lorentz-polarization and absorption corrections were made.

The structure was solved by direct methods (SHELXS program) and refined by full-matrix least-squared method (SHELXL-2014 program; G.M. Sheldrick, Acta Cryst. 2015, C71, 3-8).

The minimized function was $\sum w\left|\left|F_0\right|^2 - \left|F_c\right|^2\right|^2$ where

$$w = [\sigma^2(F_0^2) + (0.0390P)^2 + 0.4830P]^{-1} \quad P = (F_0^2 + 2F_c^2)/3.$$

All H atoms were added with idealized geometry and all C-H bond lengths were refined with the constraint that all C-H distances in a group were equal. For all CH_2 (and CH_3) groups, the H isotropic temperature factor has been calculated equal to 1.2 (and 1.5) times the equivalent temperature factor of the atom to which they are linked. The final *R* factors are shown in Table SI-1 together with other details of the quality of the molecule structure.

Figures

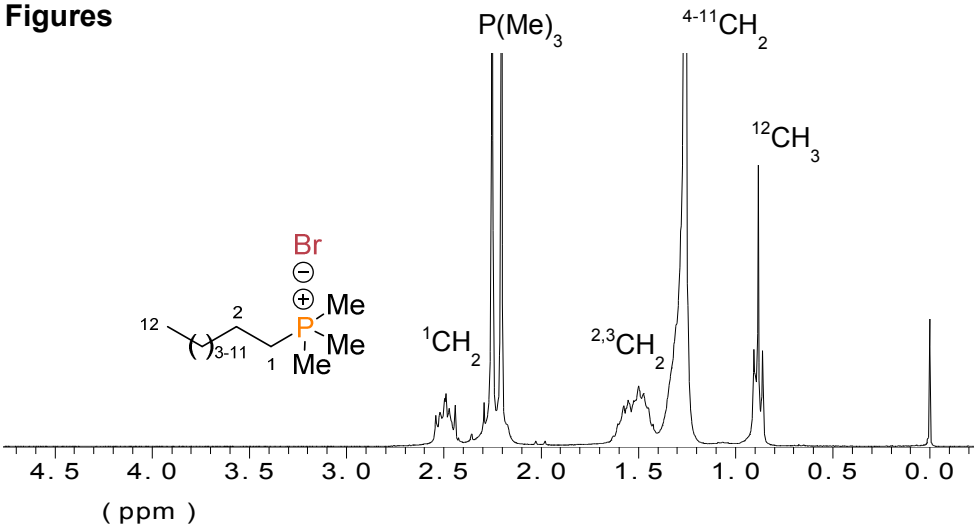
P(Me)3
4-11CH2
12CH3
Br
Me
Me
Me
12
2
3-11
1
1CH2
2,3CH2
4.5 4.0 3.5 3.0 2.5 2.0 1.5 1.0 0.5 0.0
(ppm)

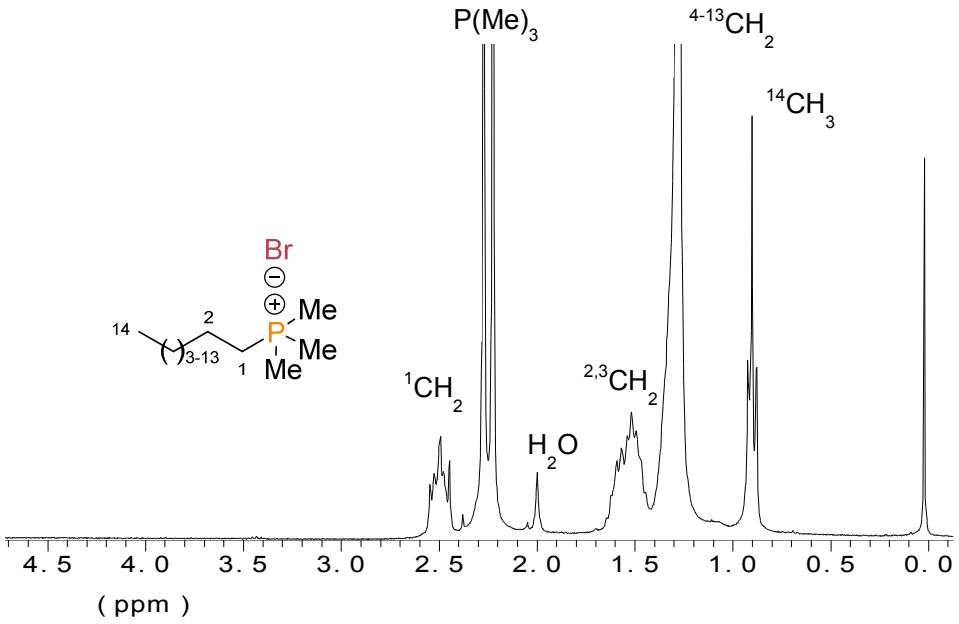
P(Me)3
4-13CH2
14CH3
Br
Me
Me
Me
14
2
3-13
1
1CH2
H2O
2,3CH2
4.5 4.0 3.5 3.0 2.5 2.0 1.5 1.0 0.5 0.0
(ppm)

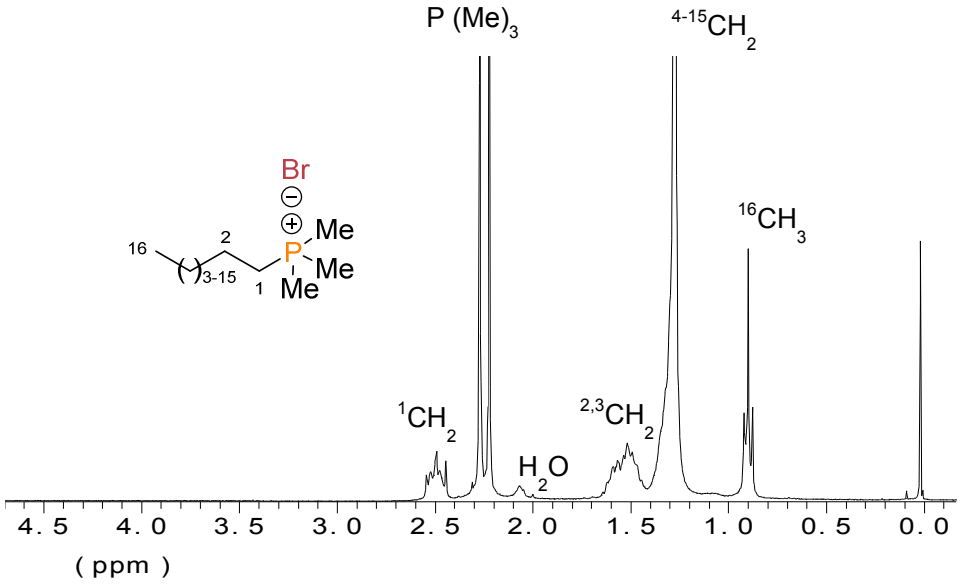
P (Me)3
4-15CH2
16CH3
Br
Me
Me
Me
16
2
3-15
1
1CH2
H2O
2,3CH2
4.5 4.0 3.5 3.0 2.5 2.0 1.5 1.0 0.5 0.0
(ppm)

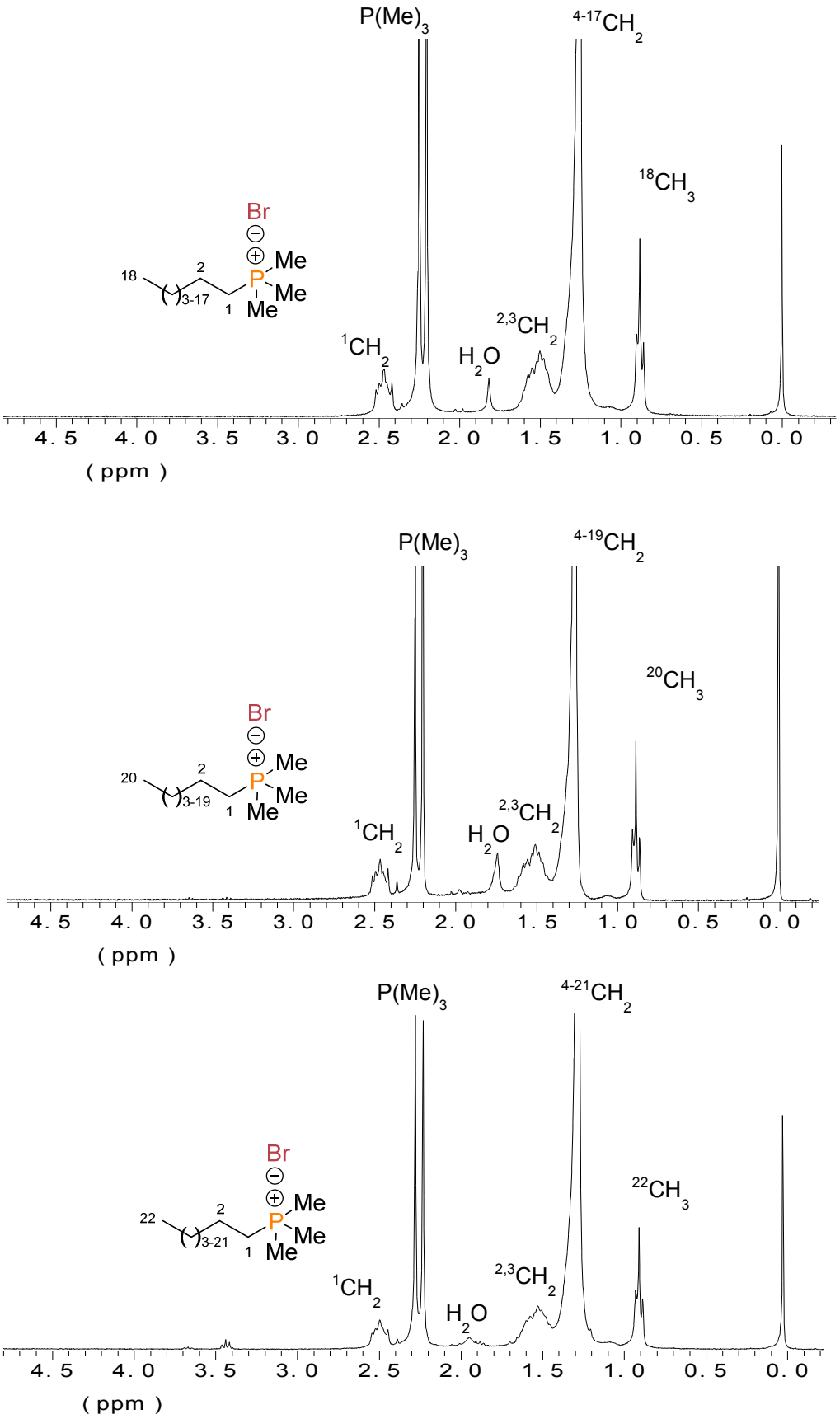

Fig. SI-1. ^{1}H NMR spectra of *n*ATMP·Br surfactants.

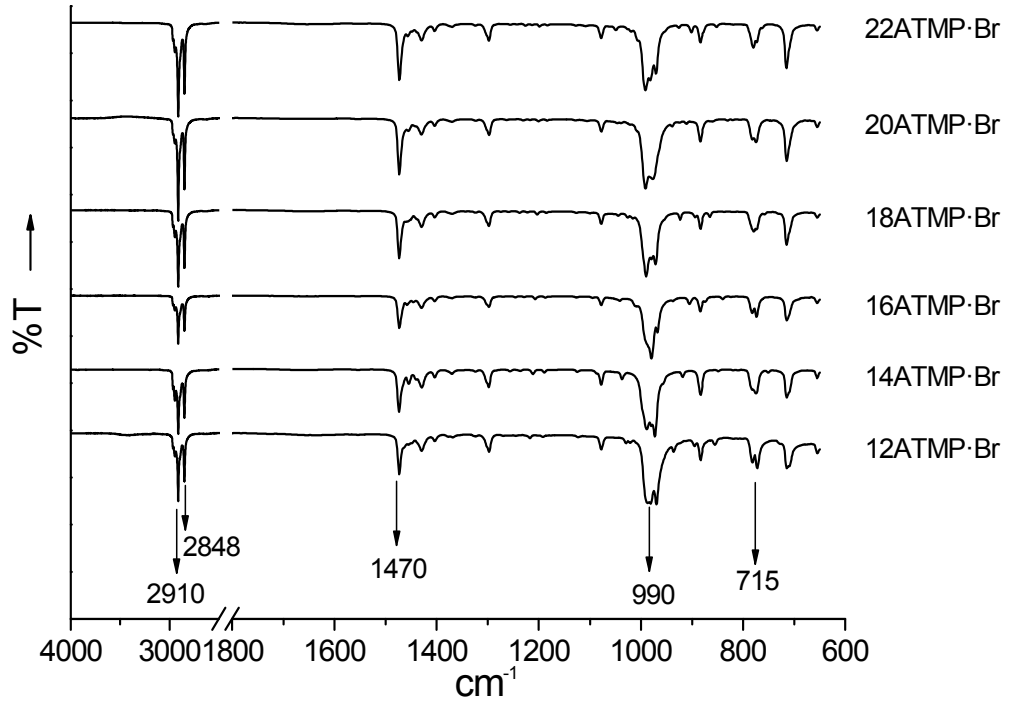

Fig. SI-2. Comparison of FT-IR spectra of *n*ATMP·Br surfactants.

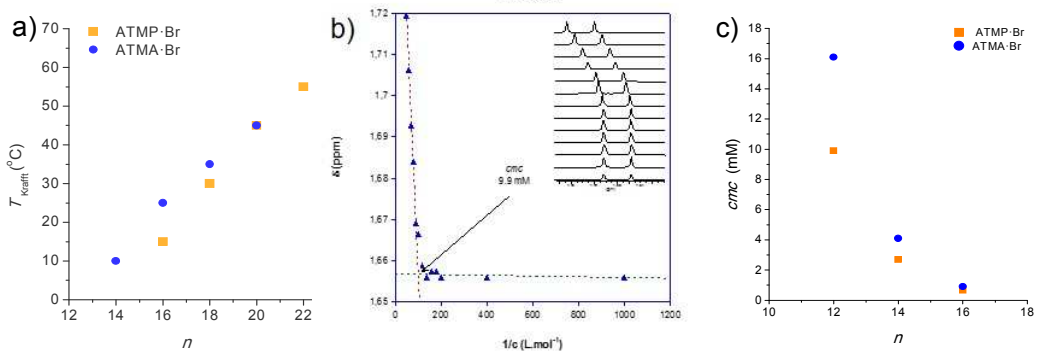

Fig. SI-3. Comparison of the above 0 ºC Krafft temperatures for *n*ATMP·Br and *n*ATMA·Br surfactants (a), plot of the methyl chemical shift of 12ATMP·Br against concentration at 25 ºC with indication of the *cmc*; inset: the evolution of the ^{1}H NMR methyl signal of 12ATMP·Br with concentration (b) and comparison of the *cmc* determined by ^{1}H NMR for *n*ATMP·Br and *n*ATMA·Br with *n*=12, 14 and 16 (c).

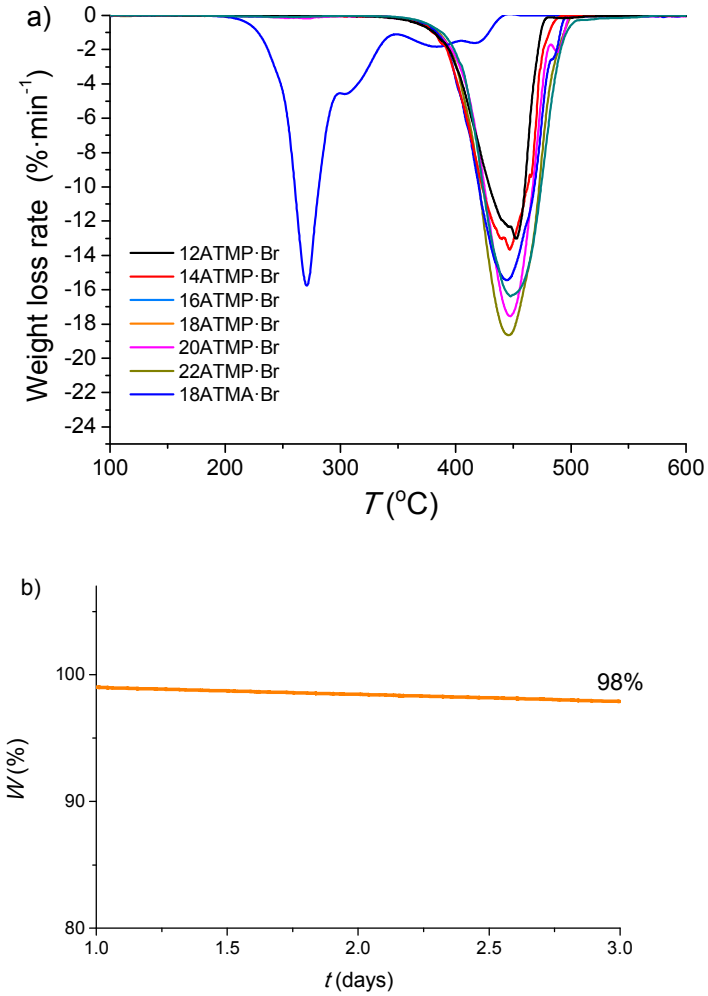

Fig. SI-4. TGA derivative curves of *n*ATMP·Br surfactants (a). Isothermal essay realized with 18ATMP·Br at 280 ºC (b).

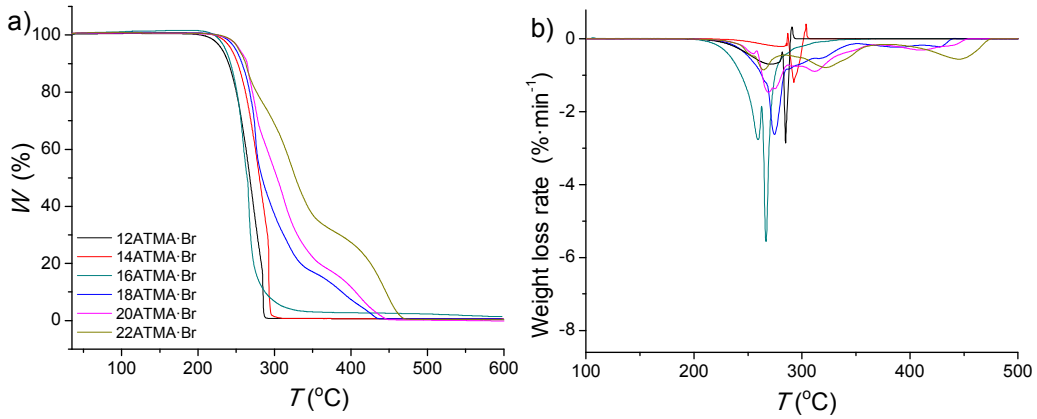

Fig. SI-5. TGA traces of *n*ATMA·Br recorded under a nitrogen atmosphere (a) and their corresponding derivative curves (b).

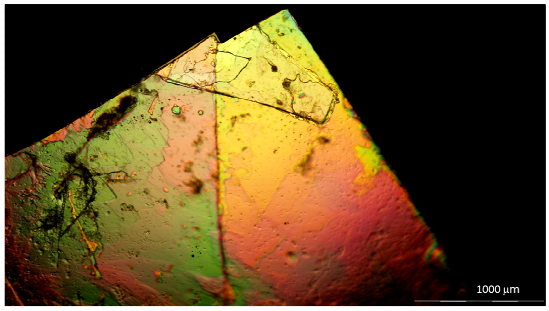

Fig. SI-6. Optical micrograph recorded from the single-crystal of 12ATMP·Br which was obtained by vapor diffusion technique and used for XRD analysis.

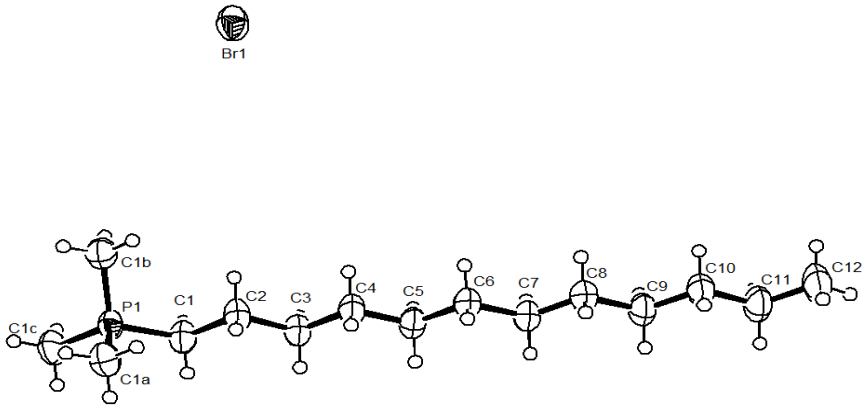

Fig. SI-7. ORTEP representation of the 12ATMP·Br molecule in the conformation adopted in the crystal with atom labelling indication. The displacement ellipsoids are drawn at 50% probability levels and H atoms are drawn as small empty circles of arbitrary radius.

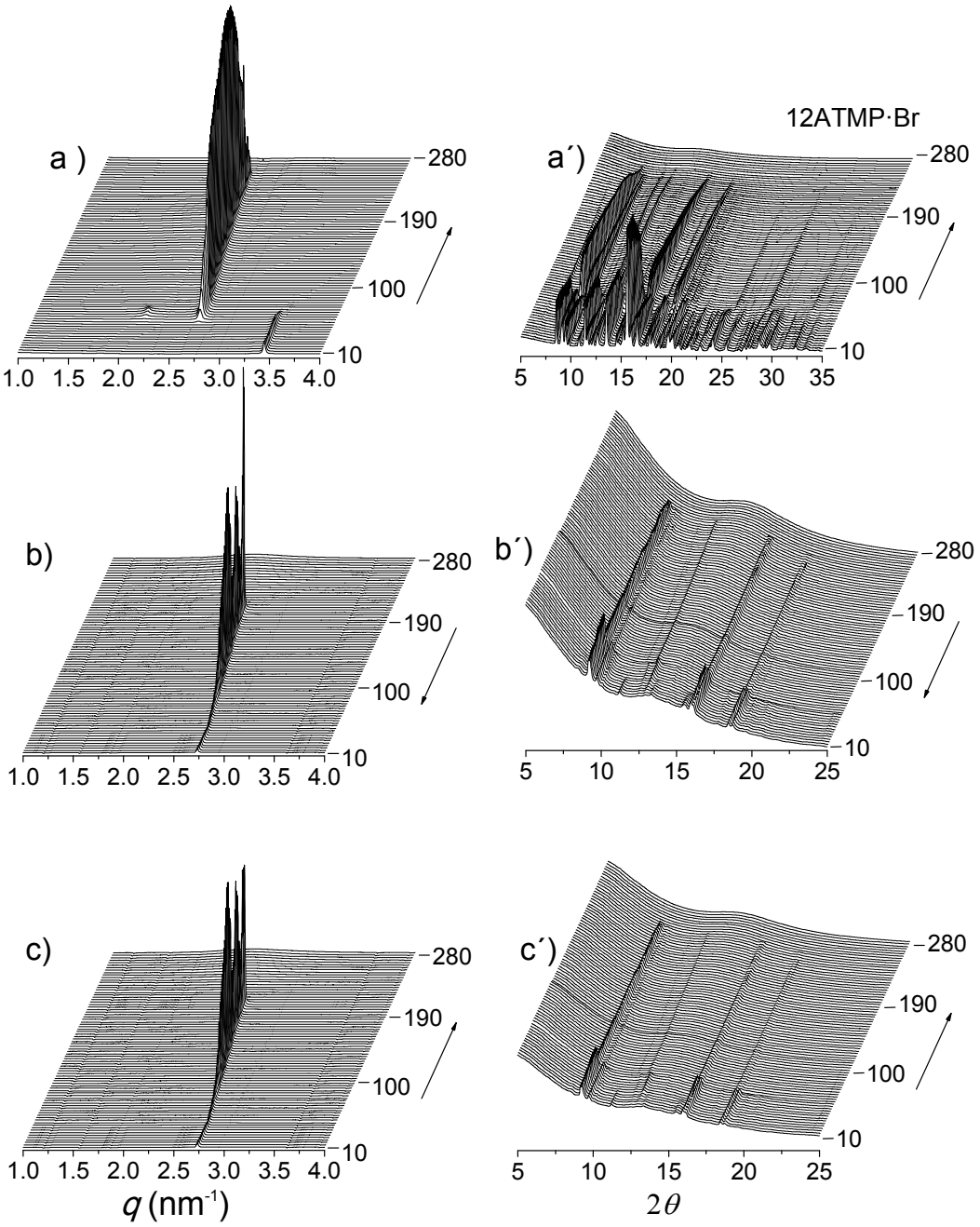

Fig. SI-8. SAXS (left) and WAXS (right) plots from 12ATMP·Br registered over the 10-280 ºC interval. a) heating, b) cooling and c) reheating.

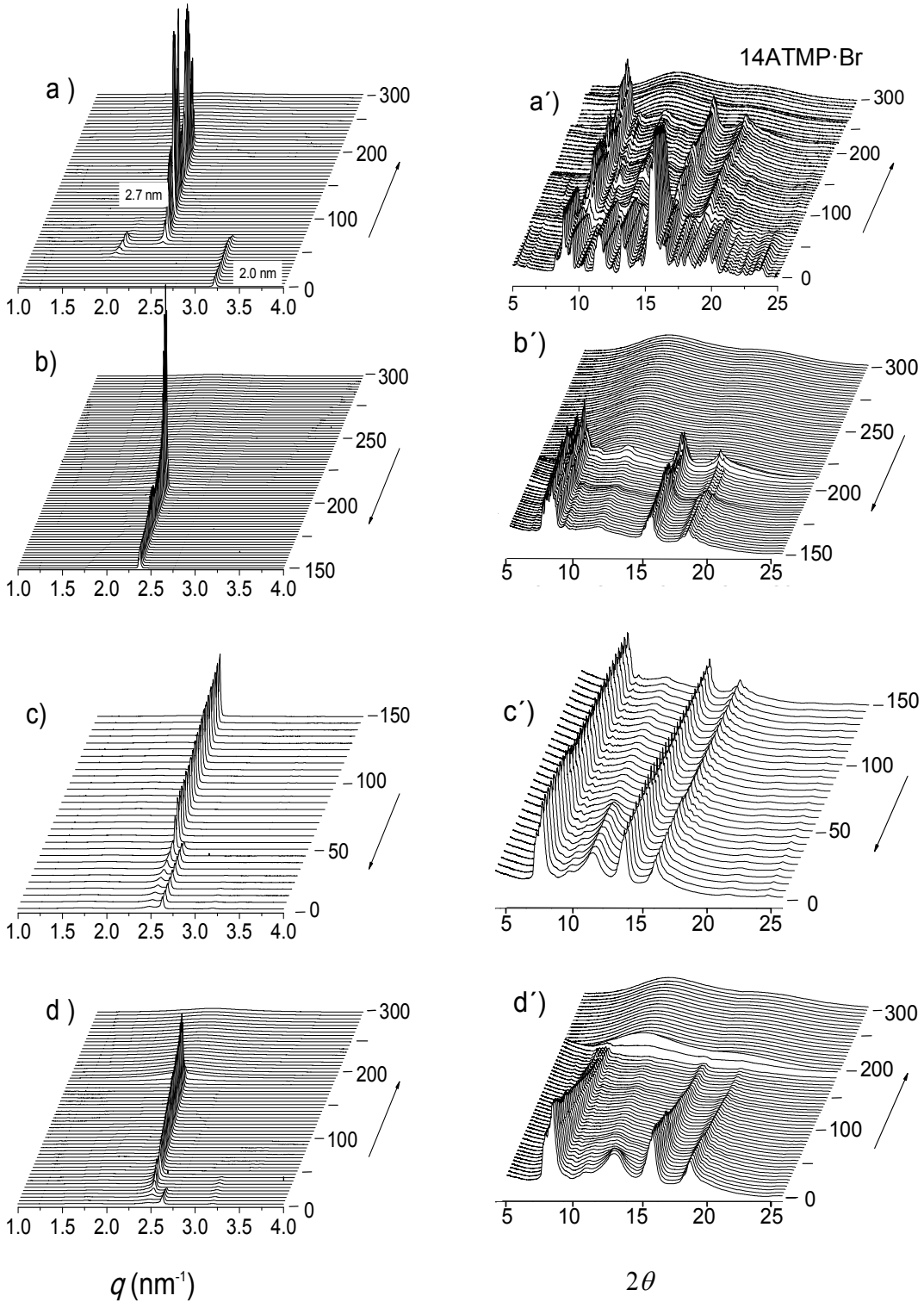

Fig. SI-9. SAXS (left) and WAXS (right) plots from 14ATMP·Br registered over the 0-300 ºC interval. a) heating, b) slow cooling, c) fast cooling and d) reheating.

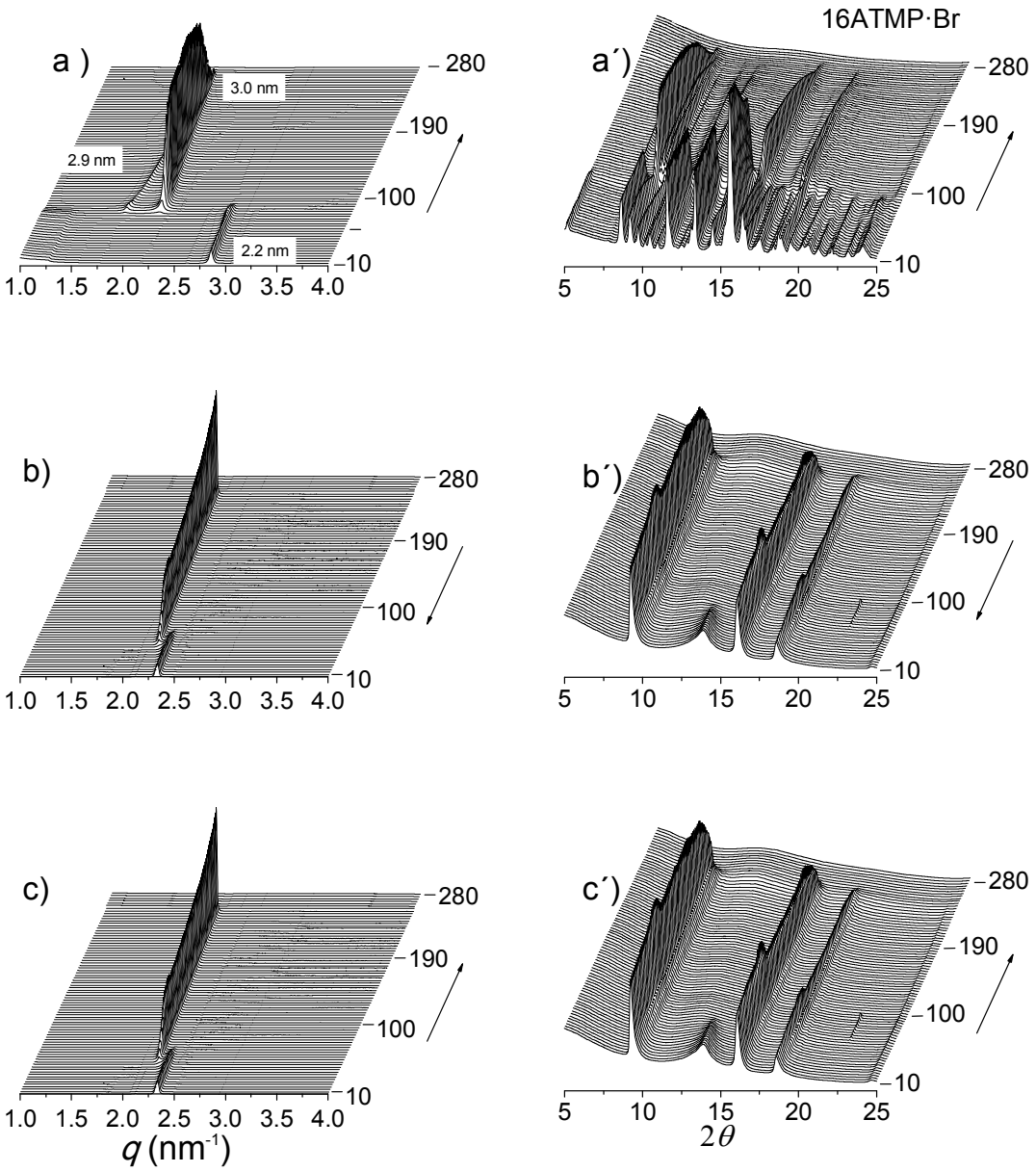

Fig. SI-10. SAXS (left) and WAXS (right) plots from 16ATMP·Br registered over the 10-280 ºC interval. a) heating, b) cooling and c) reheating.

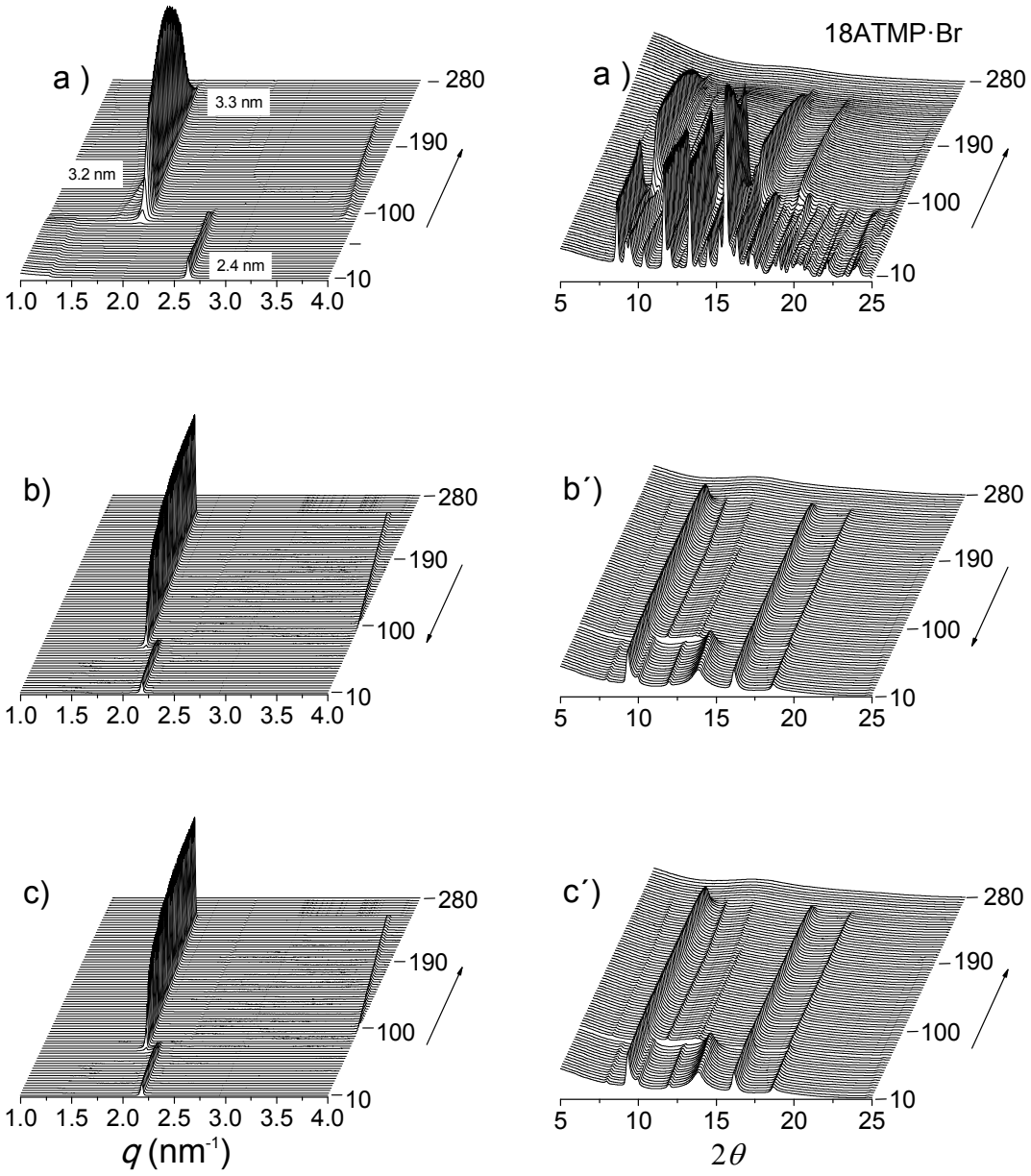

Fig. SI-11. SAXS (left) and WAXS (right) plots from 18ATMP·Br registered over the 10-280 ºC interval. a) heating, b) cooling and c) reheating.

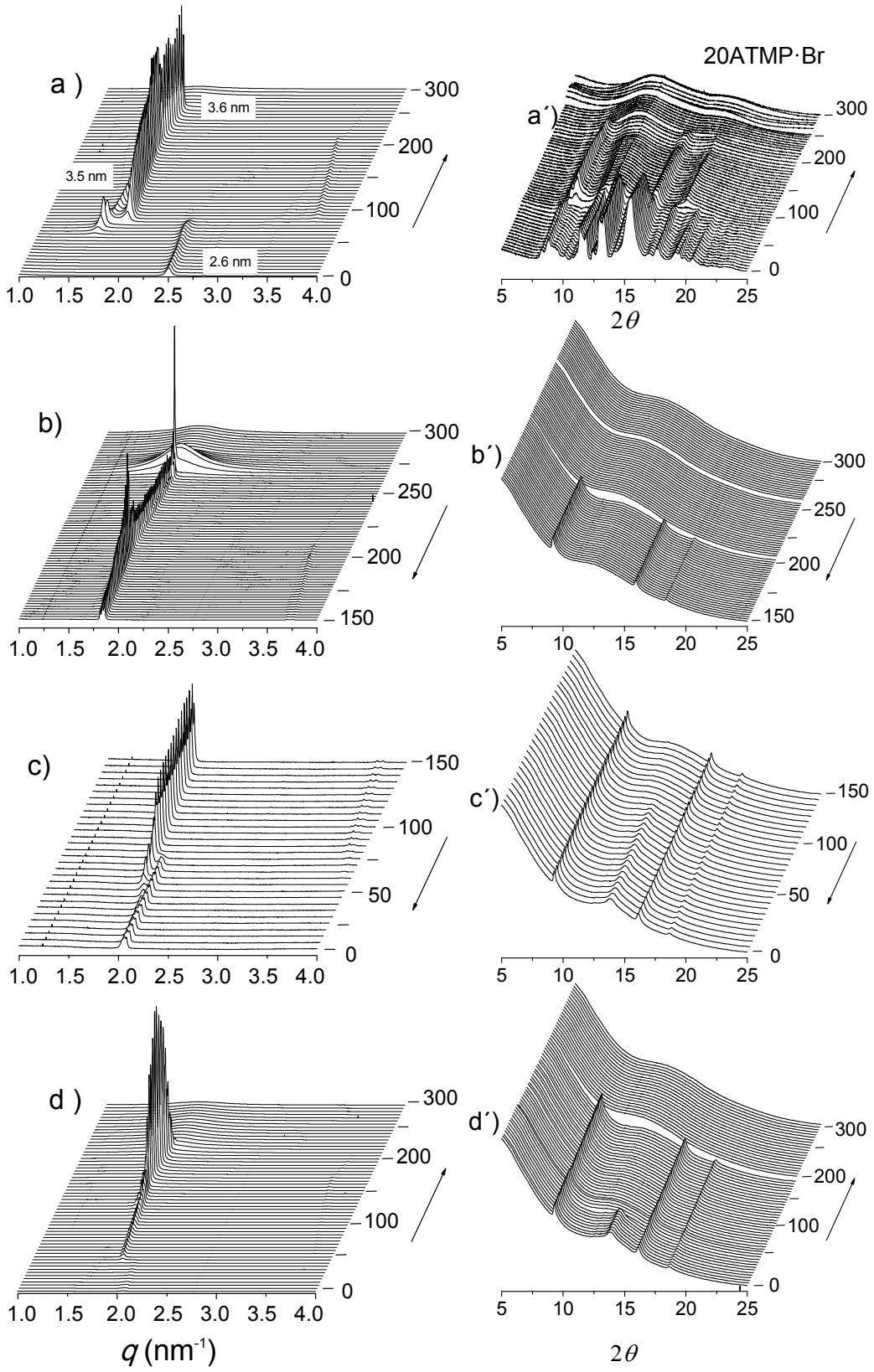

Fig. SI-12. SAXS (left) and WAXS (right) plots from 20ATMP·Br registered over the 0-300 ºC interval. a) heating, b) slow cooling, c) fast cooling and d) reheating.

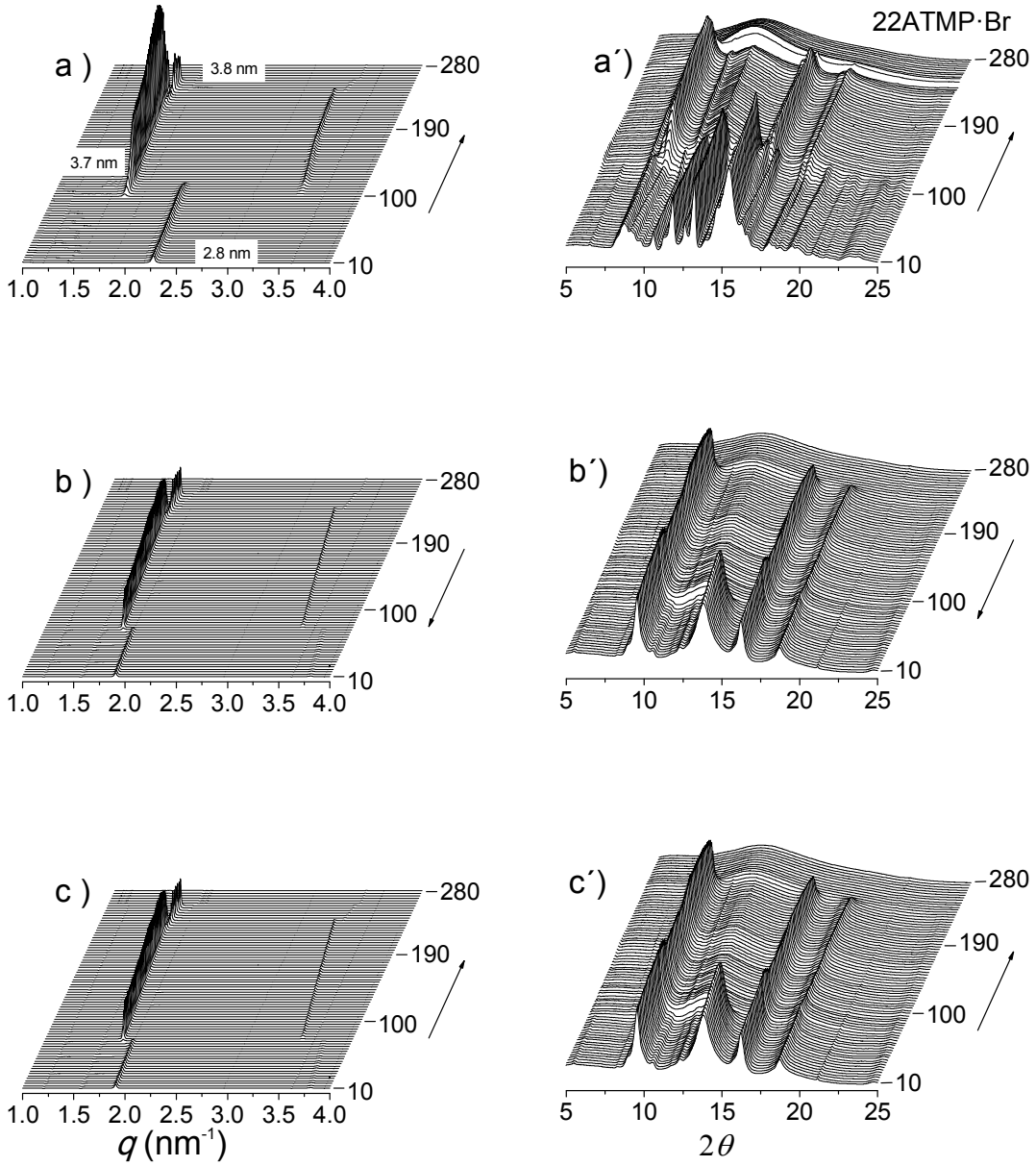

Fig. SI-13. SAXS (left) and WAXS (right) plots from 22ATMP·Br registered over the 10-280 ºC interval. a) heating, b) cooling and c) reheating.

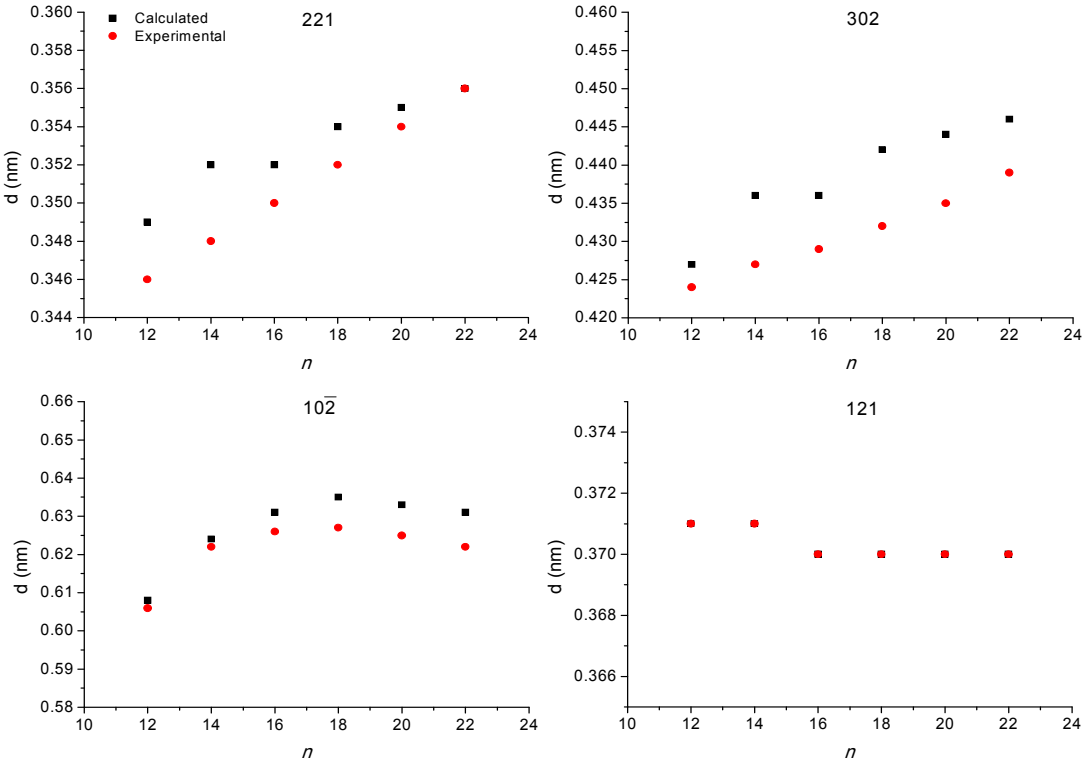

Fig. SI-14. Graphical comparison of the observed (at 25 ºC) and calculated main *d*-spacings (nm) with $h \neq 0$ for *n*ATMP·Br.

12ATMP·Br

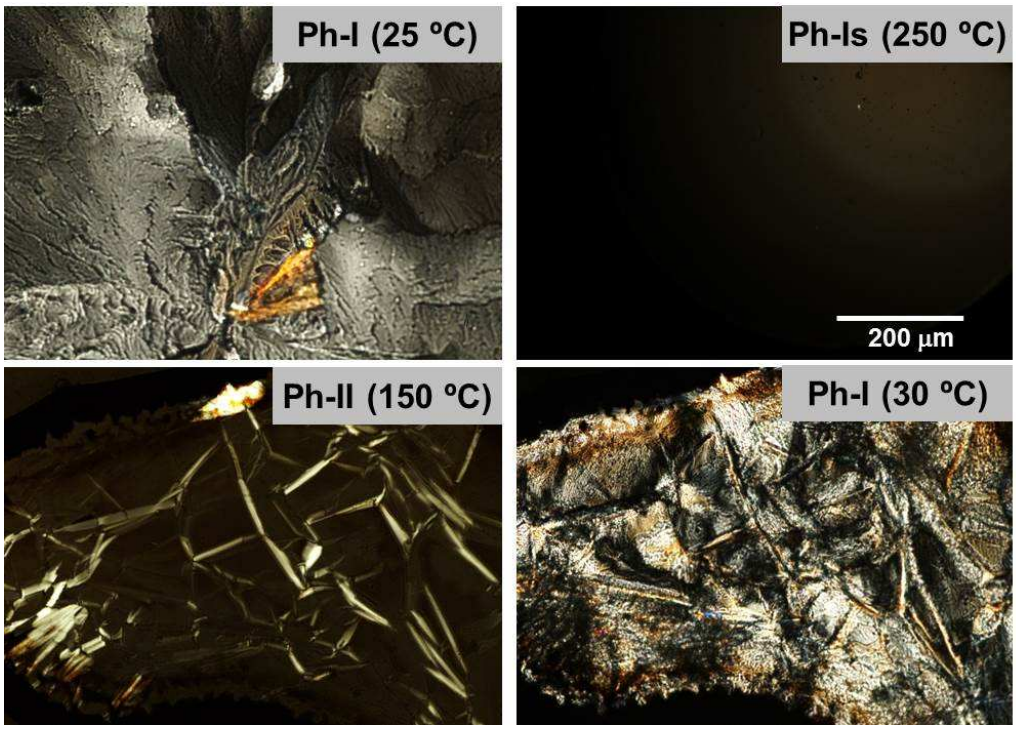

16ATMP·Br

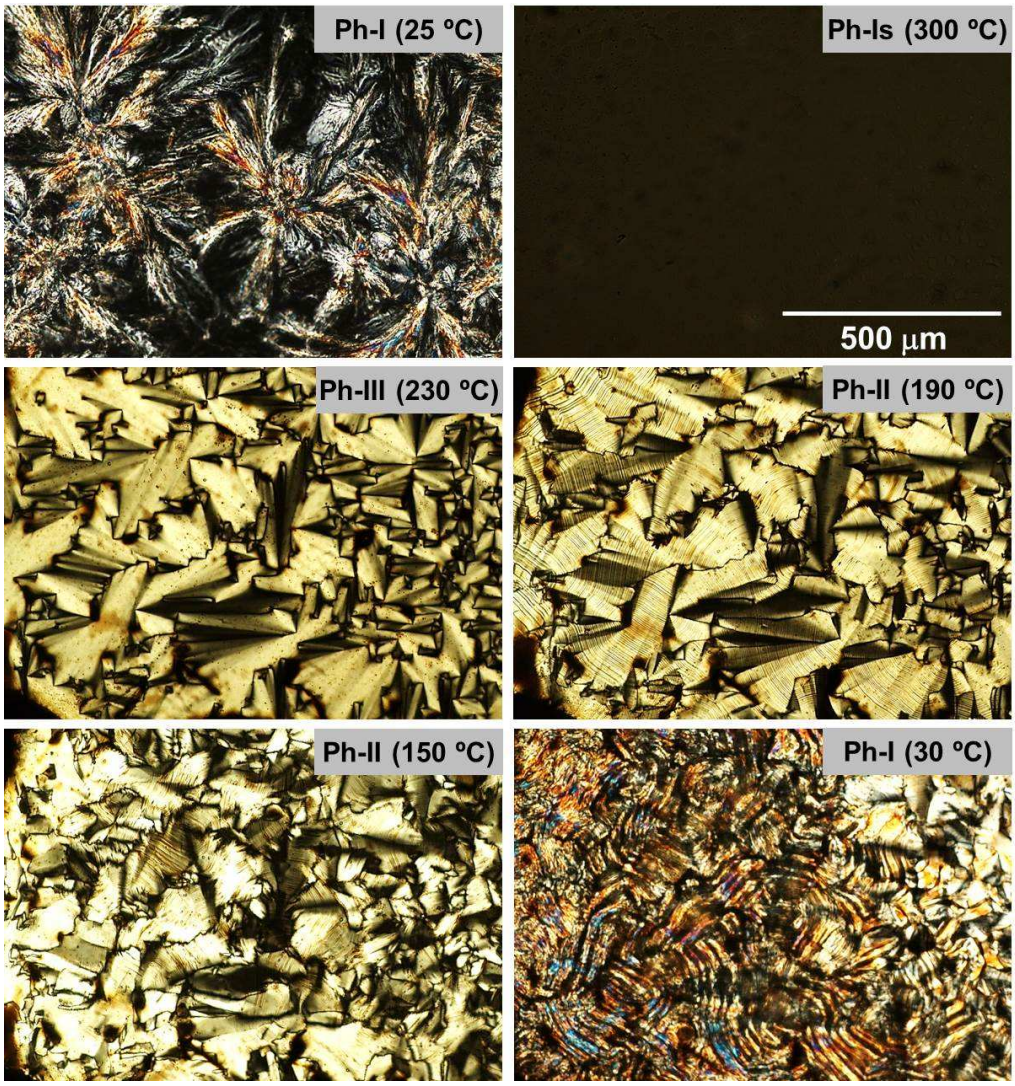
Ph-I (25 ºC)
Ph-Is (300 ºC)
500 μm
Ph-III (230 ºC)
Ph-II (190 ºC)
Ph-II (150 ºC)
Ph-I (30 ºC)

18ATMP·Br

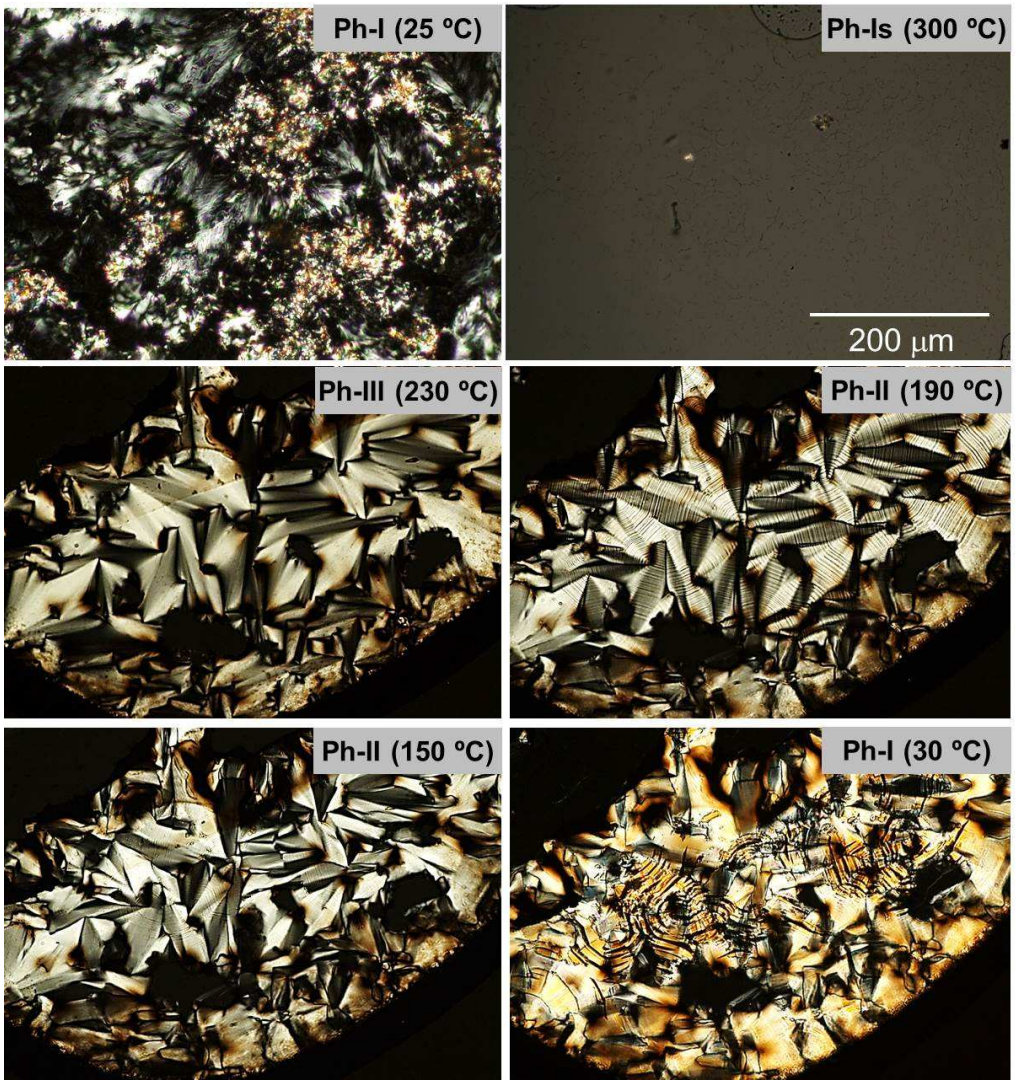
Ph-I (25 ºC)
Ph-Is (300 ºC)
200 μm
Ph-III (230 ºC)
Ph-II (190 ºC)
Ph-II (150 ºC)
Ph-I (30 ºC)

22ATMP·Br

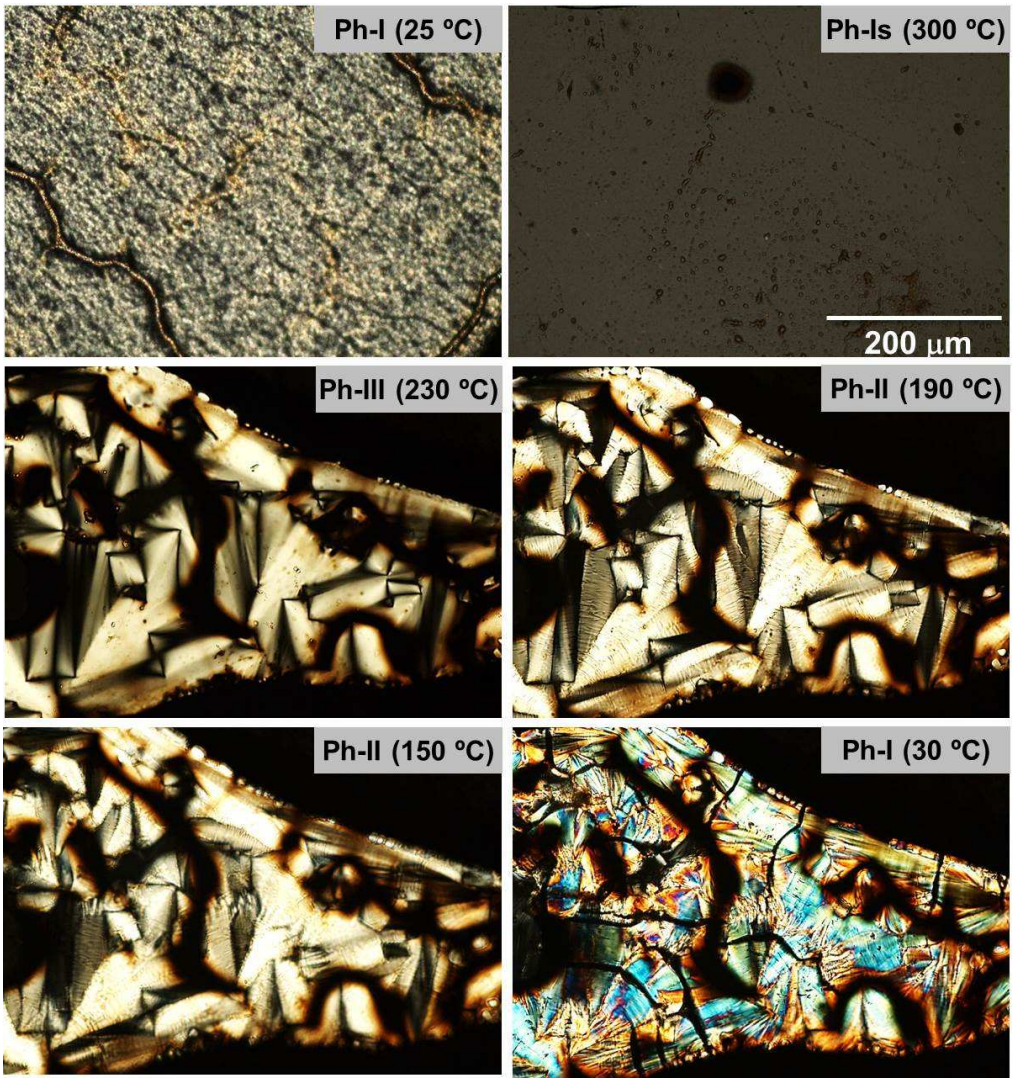

Fig. SI-15. POM micrographs recorded from *n*ATMP·Br at the indicated temperatures.

Tables

Table SI-1. Crystal data and structure refinement for 12ATMP·Br.

Empirical formula	C_{15} H_{34} Br P
Formula weight	325.30
Temperature	293(2) K
Wavelength	0.071073 nm
Crystal system, space group	Monoclinic, P 2_1/c
Unit cell dimensions	*a* = 1.82906(10) nm alpha = 90º *b* = 0.79655(4) nm beta = 93.119(2)º *c* = 1.26721(7) nm gamma = 90º
Volume	1843.51(17) Å^3
Z, Calculated density	4, 1.172 Mg/m^3
Absorption coefficient	2.301 mm^{-1}
F(000)	696
Crystal size	0.449 x 0.139 x 0.098 mm
Theta range for data collection	2.230 to 25.393º
Limiting indices	-22<=*h*<=22, -9<=*k*<=9, -15<=*l*<=15
Reflections collected / unique	25175 / 3385 [*R*(int) = 0.0429]
Completeness to theta = 25.242	99.9 %
Absorption correction	Semi-empirical from equivalents
Max. and min. transmission	0.7452 and 0.6345
Refinement method	Full-matrix least-squares on F^2
Data / restraints / parameters	3385 /0/169
Goodness-of-fit on F^2	1.046
Final *R* indices [I>2σ (I)]	*R*1 = 0.0298, w*R*2 = 0.0720
R indices (all data)	*R*1 = 0.0480, w*R*2 = 0.0814
Extinction coefficient	n/a
Largest diff. peak and hole	0.329 and -0.255 e.Å^{-3}

Table SI-2. Atomic coordinates (x 10^4) and equivalent isotropic displacement parameters (Å ^{2} x 10^3) for 12ATMP·Br. U (eq) is defined as one third of the trace of the orthogonalized Uij tensor.

Atom	x	y	z	U(eq)
Br(1)	1173(1)	830(1)	3176(1)	64(1)
P(1)	1077(1)	9047(1)	6693(1)	44(1)
C(1)	2051(1)	8920(3)	6601(2)	53(1)
C(2)	2286(1)	8825(3)	5469(2)	53(1)
C(3)	3109(1)	8874(3)	5373(2)	52(1)
C(4)	3318(1)	8836(3)	4230(2)	53(1)
C(5)	4135(1)	8870(3)	4091(2)	54(1)
C(6)	4340(1)	8855(3)	2952(2)	52(1)
C(7)	5158(1)	8870(3)	2808(2)	54(1)
C(8)	5366(1)	8861(3)	1673(2)	55(1)
C(9)	6188(1)	8880(3)	1543(2)	56(1)
C(10)	6405(1)	8870(3)	408(2)	58(1)
C(11)	7220(2)	8917(3)	286(2)	68(1)
C(12)	7431(2)	8903(4)	-854(3)	96(1)
C(1A)	735(1)	10919(3)	6096(2)	57(1)
C(1B)	654(1)	7295(3)	6042(2)	58(1)
C(1C)	874(2)	9030(4)	8051(2)	60(1)

Table SI-3. Torsion angles (º) for 12ATMP·Br.

C(1A)-P(1)-C(1)-C(2)	-63.2(2)
C(1B)-P(1)-C(1)-C(2)	57.0(2)
C(1C)-P(1)-C(1)-C(2)	176.72(19)
P(1)-C(1)-C(2)-C(3)	174.81(18)
C(1)-C(2)-C(3)-C(4)	-178.1(2)
C(2)-C(3)-C(4)-C(5)	-179.6(2)
C(3)-C(4)-C(5)-C(6)	-179.2(2)
C(4)-C(5)-C(6)-C(7)	-179.4(2)
C(5)-C(6)-C(7)-C(8)	-179.8(2)
C(6)-C(7)-C(8)-C(9)	179.9(2)
C(7)-C(8)-C(9)-C(10)	179.9(2)
C(8)-C(9)-C(10)-C(11)	179.1(2)
C(9)-C(10)-C(11)-C(12)	179.9(2)

Table SI-4. Crystallographic *a* and β values of the *n*ATMP·Br salts used for the simulations of the crystal lattices to obtain their respective SAXS and WAXS profiles.

*n*ATMP·Br	[b]*a* (nm)	β (º)
[a]12	1.83	93.1
14	2.05	97.0
16	2.25	101.0
18	2.47	103.5
20	2.70	106.0
22	2.92	108.0

[a]*a* and β values of 12ATMP·Br are based on the experimental results of 12ATMP·Br.

[b]*b* and *c* parameters and α and γ angles of all the cells are fixed (*b* =0.7965 and *c* = 1.2672 nm, $\alpha = \gamma = 90º$), according to the experimental result of 12ATMP·Br.